Developing a Genetic Model for Puerto Rico's Tibes Iron Deposit through Field Observations and Geochemical Analyses

By

Marisa Barefoot

A thesis submitted to the Graduate Faculty of
Auburn University
in partial fulfilment of the
requirements of the degree of
Master of Science

Auburn, Alabama
December 11, 2021

Approved by

Laura D. Bilenker, Chair, Assistant Professor of Geosciences
Thomas Hudgins, Associate Professor of Geology, University of Puerto Rico, Mayagüez
Willis Hames, Professor of Geosciences

Abstract

Understanding the formation of iron deposits is key for locating new resources and upholding our pledge to transition to renewable energy as iron is required to make steel, a critical component of all green energy technologies. Puerto Rico's dynamic geologic history produced a wealth of ore deposits, including the Tibes iron skarn near Ponce. Linear massive magnetite bodies have sharp contacts with the host rock and orientations similar to local faulting, indicating lithologic and/or structural control(s) on ore deposition. The whole rock mineralogy and trace element (Ca, Al, Mn, Ti, V) concentrations of Tibes magnetite are consistent with the limited existing data from iron skarns. Variations in the concentrations of these elements correlate with the proximity of each ore body to the Tibes diorite. Isotope analyses of Tibes magnetite reveal δ^{56}Fe values between 0.13-0.39‰ and δ^{18}O values between 2.83-5.02‰, indicating a magmatic source of the ore fluid with minimal meteoric input or post-depositional alteration. Compositional zonation and silicate micro-inclusions in the magnetite record multiple ore-forming events and fluctuating ore-fluid conditions. The proposed genetic model is a major step in understanding the Tibes deposit as a resource and these data provide a new framework for studying similar deposits worldwide.

Acknowledgements

I would first like to thank my advisor Dr. Bilenker. You inspired me to want to go to graduate school and supported me throughout my entire time here at Auburn. You are an exceptional person and academic, and I couldn't have done this without you. I would also like to thank my collaborators at the University of Puerto Rico, Mayagüez, Dr. Tom Hudgins and David Giovannetti-Nazario, for their help with field work and sample collection. Thank you to Dr. Hames and Dr. Billor for help with EMPA and LA-ICP-MS work. A special thank you to my friends and fellow graduate students, Elyssa Rivera, Dogancan Yasar, and Tyler Smith for helping keep me sane and for constantly supporting me. I would also like to thank my family and girlfriend Britanee Arthur for their support. And lastly I would like to thank the Geological Society of America and the Society of Economic Geologists for funding this research.

Table of Contents

List of Tables

List of Figures

1. Introduction

Puerto Rico is a Caribbean Island located on the eastern end of the Greater Antilles (Figure 1). The island has a complicated geologic and tectonic history, which has allowed for the concentration of large volumes of metals in its many different ore deposits. Due to their variable geologic origins and unusual compositions, ore deposits are valuable records of magmatic activity, metal transport, and fluid movement within the crust, in addition to being potential economic resources. These deposits hold the key to understanding Puerto Rico's dynamic and debated geologic history.

Figure 1. Map of the Caribbean Sea with the island of Puerto Rico outlined in red (modified from Google Maps).

Between 1933 and 1954, Puerto Rico enacted a series of mining laws that restricted the development of the island's mineral resources. These laws required that the island's resources be utilized only for the benefit of the Puerto Rican people and only when production would not have a negative impact on the environment. These laws also gave Puerto Rico's Secretary of

Natural Resources the power to approve or deny mining leases (Gelabert, 2011). As a result, Puerto Rico is currently only extracting cement and lime from its open-pit quarries, leaving the majority of its mineral resources completely untapped and, therefore, grossly understudied (U.S. Geological Survey, 2019).

Puerto Rico's iron deposits in particular have the potential to contribute greatly to our understanding of the geologic history of the island, and three have been identified. The two well-known Puerto Rican iron deposit localities are the Keystone Mine and the Island Queen Mine on the northeast area of the island (Bawiec et al., 1998). Between 1951-1953, these mines produced a combined 220,000 tons of ore with an Fe content greater than 60% (Vazquez, 1960). The Tibes iron prospect near Ponce also hosts large volumes of iron ore, but since there is no economic motivation for exploration, little work has been done to study it. All three of these iron deposits have been classified by early geologic mapping efforts as skarns, which form as a result of a magmatic intrusion into carbonate rock and described in detail in section 5.

2. Objectives

The main objective of this study is to characterize Tibes magnetite ore in detail in order to produce a genetic model of the Tibes iron deposit. To accomplish this, we must combine field and geochemical observations to identify both the source and composition of the iron ore bodies present at the deposit. As a result, we will be able to add the Tibes skarn deposit to global databases, provide Puerto Rico with valuable information about their mineral resources, and assess the application of newer geochemical techniques, like Fe isotopes, to skarns. Iron is a vital societal commodity as it is used to make steel and plays an important role in green energy technologies like wind turbines and solar panel farms. Understanding how iron skarns

form is key for finding new iron deposits and building the resources we need to transition toward utilizing more renewable technology.

3. Geology and Tectonic Setting of Puerto Rico

Puerto Rico is a seismically active area with a dynamic tectonic history that continues to be debated. The oldest rocks in Puerto Rico are Jurassic volcanic rocks thought to have been formed in an island arc off of the west coast of South America near the latitude of the current day Peru-Ecuador border (Elston & Krushensky, 1983). Volcanism continued and was followed by the intrusion of Late Cretaceous to Early Tertiary felsic and mafic magmas (Schellekens, 1998). These volcanic and plutonic rocks are combined into a group called the "older complex" (Kaye, 1957). The island arc moved north then east during the Eocene to Miocene to its present-day position between the North and South American plates. This movement was accompanied by a clockwise rotation of >90° (Krushensky & Schellekens, 2001). Though many aspects of the geologic and tectonic history of the Caribbean and the Greater Antilles are generally agreed upon, the exact degree of plate motion and interactions are still debated (e.g., Dolan et al., 1991; Jolly et al., 1998; Pindell, 1994; Pindell et al., 2006).

Puerto Rico is part of the Puerto Rico-Virgin Islands (PRVI) microplate, which sits at the Caribbean-North American plate boundary (Schellekens, 1998; Figure 2). In its current position, the PRVI microplate is experiencing left-lateral motion along the North American plate boundary (Krushensky & Schellekens, 2001). It has been debated whether this boundary reflects a purely strike-slip relationship between the North American and Caribbean plates (Minster & Jordan, 1978) or if there is oblique underthrusting (Sykes et al., 1982). Through the use of long-range side scan sonar images and seismic reflection data, Masson and Scanlon

(1991) were able to identify this relationship as almost purely strike-slip along the Puerto Rico Trench (between 65.5°W and 68°W) even though there is prevalent underthrusting to the east and west. This motion has resulted in the counterclockwise rotation of the PRVI microplate (Krushensky & Schellekens, 2001). The effects of this rotation are exemplified by the extensional setting of the Mona Canyon (Speed & Larue, 1991) and Anegada Passage (Larue, 1990) to the west and east of Puerto Rico respectively, and by the thrusting in the Muertos Trough to the south (Figure 2; Byrne et al., 1985).

This movement also resulted in the extensive faulting and folding present in the older complex. These igneous rocks are characterized by northwest-trending normal faulting, as illustrated in Figure 3 (Jolly et al., 1998). The older complex is overlain by the middle Tertiary

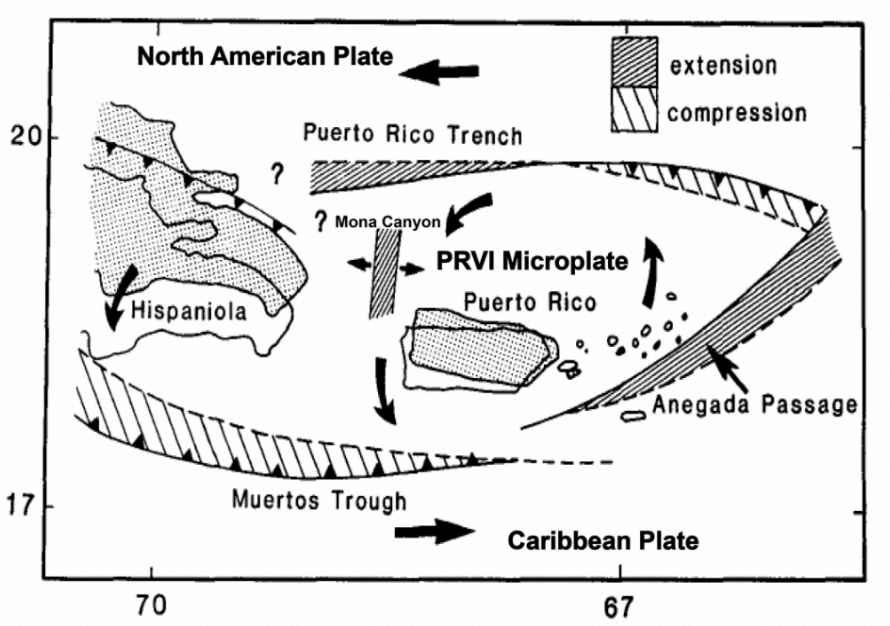

Figure 2. Model illustrating the plate interactions around Puerto Rico and the resulting counter-clockwise motion of the Puerto Rico-Virgin Island (PRVI) microplate. Stippled areas indicate previous positions while non-stippled areas indicate the current positions (modified from Masson & Scanlon, 1991).

sequence, which consists of late Oligocene calcareous marine sediments with no associated volcanic activity. There is minimal structural deformation present in the middle Tertiary sequence compared to the older complex (Kaye, 1957).

Puerto Rico has been divided into three main provinces based on differences in stratigraphy, lithology, and geochemistry. These provinces are the Southwest Igneous Province (SIP), the Central Igneous Province (CIP), and the Northeast Igneous Province (NIP), as illustrated in Figure 3 (Jolly et al., 1998; Krushensky & Schellekens, 2001). The SIP has some of the oldest rocks in Puerto Rico. These rocks are dominated by Jurassic and Early Cretaceous serpentinites with rafts of chert and metabasalt. They are accompanied by Cretaceous and Eocene sedimentary rocks and a northeast-southwest trending belt of Lower Tertiary intrusives and volcanics (Schellekens, 1998). The CIP primarily consists of stratified Early Cretaceous to Eocene rocks that were crosscut by felsic intrusions during the Late Cretaceous. These intrusions include the San Lorenzo batholith and the Utuado, Ciales, and Morovis plutons (Schellekens, 1998 and references therein). The CIP is separated from the NIP by the San Franciso-Cerro Mula (SFCM) fault (Figure 3). The NIP reflects a high volume of igneous activity and includes volcanic rocks as well as Cretaceous-Tertiary felsic intrusions and younger Tertiary mafic intrusions. The igneous core of the island is bounded on the north and south by relatively undisturbed Oligocene to Pliocene sedimentary rocks (Schellekens, 1998). Puerto Rico's complicated igneous and tectonic history created the perfect environment for the

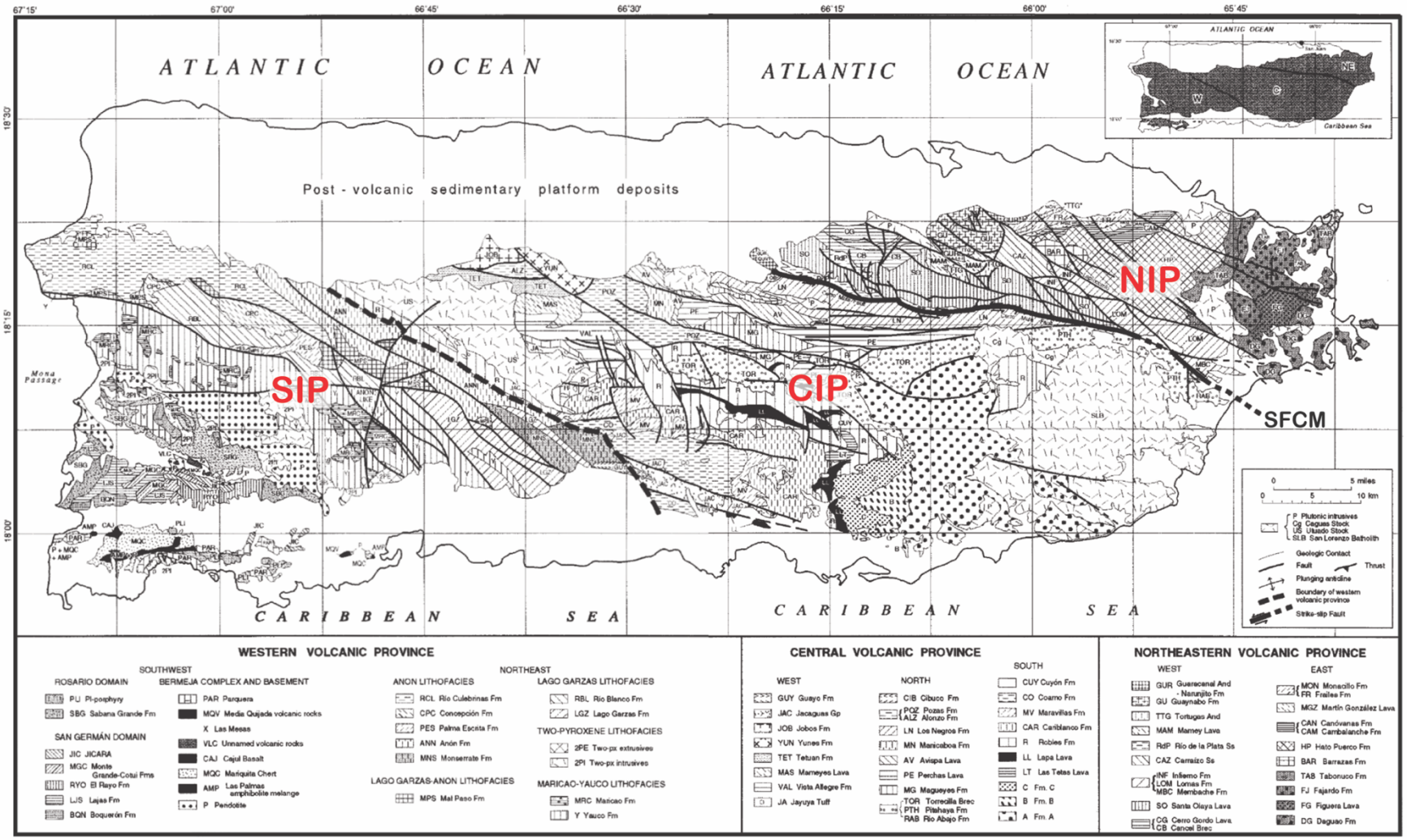

Figure 3. Geologic map of Puerto Rico depicting the Southwest Igneous Province (SIP), Central Igneous Province (CIP), and the Northeast Igneous Province (NIP). SFCM = San Franciso-Cerro Mula fault (modified from Jolly et al., 1998).

concentration of economically important metals such as iron, copper, and gold (Cox & Briggs, 1973).

4. The Ore Deposits of Puerto Rico

Even though Puerto Rico hosts a variety of ore deposits resulting from multistage tectonic activity, little research has been done to understand their characteristics, formation, and timing. Many of these deposits are associated with Cretaceous felsic intrusions like the San Lorenzo batholith in southeastern Puerto Rico and the Utuado batholith in central Puerto Rico (Figure 4; Bawiec et al., 1999). The San Lorenzo batholith is associated with both copper and iron skarns, including the Keystone and Island Queen iron skarns (Bawiec et al., 1998; Cox & Briggs, 1973). Puerto Rico's copper and copper-gold porphyry deposits are associated with younger Eocene intrusions dominated by tonalite to monzogranite stocks (Bawiec et al., 1999; Nelson et al., 2011 and references therein). These stocks surround the Utuado batholith and are some of the youngest igneous rocks in Puerto Rico (Nelson et al., 2011). This late igneous activity is crucial because it resulted in the copper mineralization of the Tanamá and Río Víví porphyry deposits (Bawiec et al., 1998). The Tanamá and Río Víví deposits contain an estimated 139 million tonnes and 104 million tonnes of ore, respectively (Lutjen, 1971).

Marine volcaniclastics were deposited around Puerto Rico during the same time as the intrusive activity (Bawiec et al., 1999) and is linked to the formation of volcanogenic manganese deposits. Subsequent weathering has produced placer gold, titanium, and platinum group element deposits as well as lateritic nickel deposits from the weathering of ultramafic dunites and peridotites (Bawiec et al., 1999).

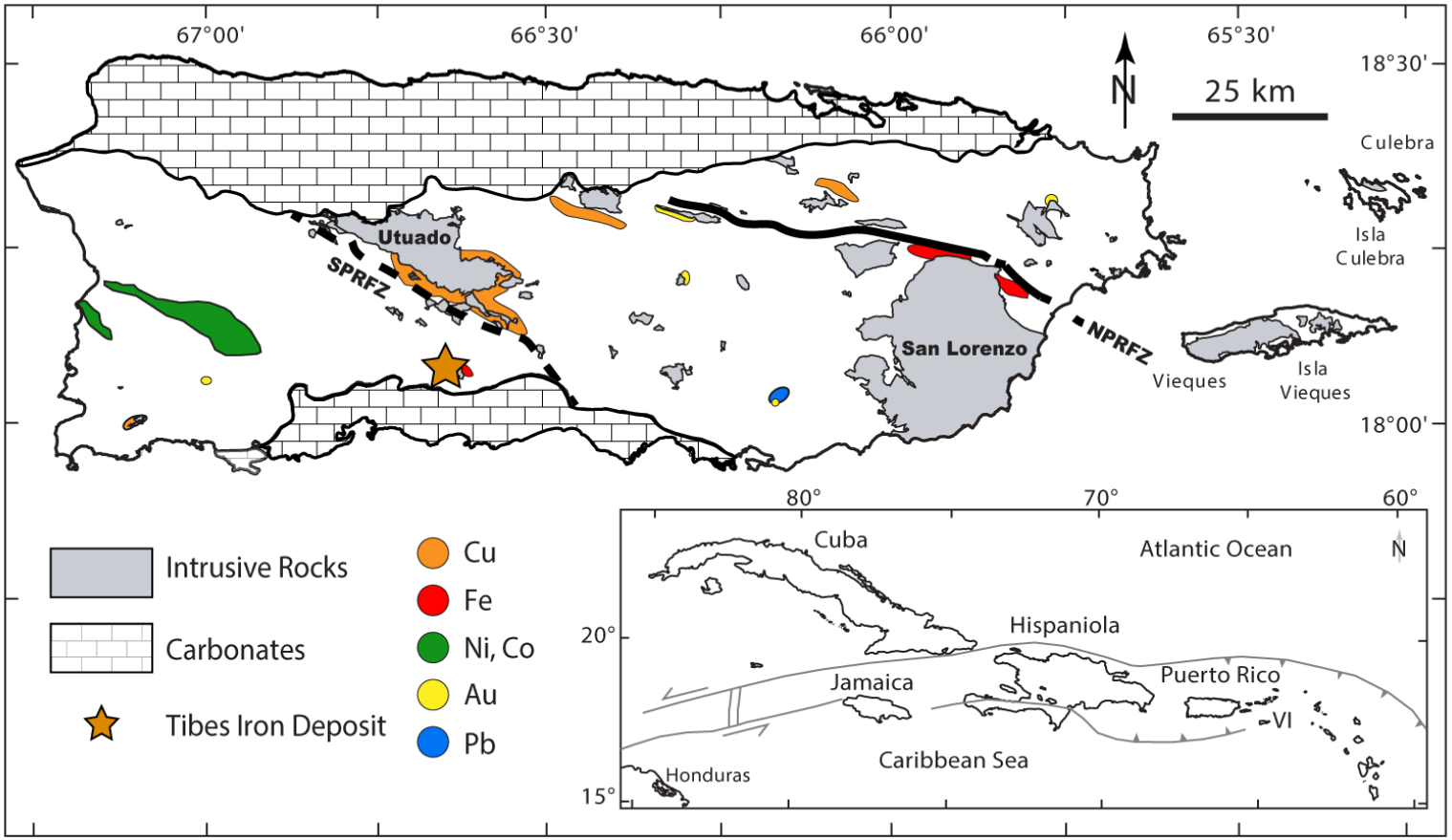

Figure 4. Map of Puerto Rico depicting the major intrusive rocks (gray areas), metallogenic zones (colored areas), and carbonate rocks. The location of the Tibes iron deposit is denoted by the orange star (modified from Cox & Briggs, 1973; Schellekens, 1998; Jolly et al., 1998; Base map provided by Dr. Thomas Hudgins).

4a. The Tibes Iron Skarn

The Tibes iron skarn is located near the city of Ponce in southern Puerto Rico (Figure 4). This deposit is thought to have formed as a result of the intrusion of a hornblende diorite stock, known as the Tibes Stock, into Late Cretaceous limestone and calcareous sediments. An array of dikes branched from this intrusion and produced heat and vapors that circulated through the limestone host rock and metasomatically altered its minerals (Pujols & Cavosie, 2007). At least 16 massive magnetite bodies are present in the Tibes deposit and are the subject of recent preliminary study (Giovannetti-Nazario & Hudgins, 2019).

5. The Formation and Importance of Skarn Deposits

Skarns are characterized by their dominant mineralogy and can contain large volumes of various economic metals, including iron (Fe), gold (Au), copper (Cu), zinc (Zn), tungsten (W), molybdenum (Mo), and tin (Sn). Iron-Cu skarns are the only type that form in oceanic island-arc settings (Meinert et al., 2005 and references therein). Iron skarns form as a result of Fe-rich plutons intruding into a limestone or volcanic host rock. First, heat from the intrusion isochemically alters the host rock. This contact metamorphism results in the formation of marble from limestone. Next, vapors from the magma containing metals, such as Fe, infiltrate the host rock. As the system cools over time, meteoric water permeates through the area causing mineralization in response to further cooling and changes to pH and redox conditions. In addition to economic metals, skarn deposits are dominated by calc-silicate minerals such as wollastonite and exhibit a characteristic zoning of garnet and pyroxene minerals (Meinert et al., 2005; Robb, 2005). The mineralogy and metals present are a direct result of the properties

(redox, composition, depth) of the magmatic intrusion and host rocks (Figure 5; Meinert et al., 2005).

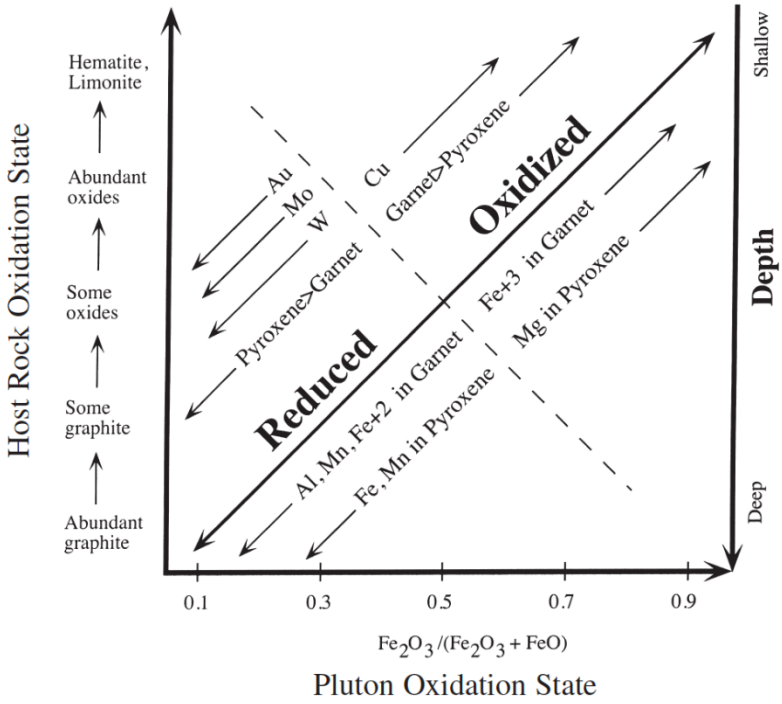

Figure 5. Comparison of host rock and pluton characteristics and the associated skarn oxidation state, which can be inferred from metal and mineral compositions (Meinert et al., 2005).

The Tibes deposit has been classified as a calcic iron skarn (Bawiec et al., 1998; Pujols & Cavosie, 2007), which generally form in oceanic island-arcs (Meinert et al., 2005). These deposits are usually found accreted to continental margins, but Puerto Rico is an unaccreted island arc, which gives us a rare opportunity to study Fe source and transport in a calcic iron skarn that has not experienced extensive post depositional metamorphism.

6. Field Observations of the Tibes Prospect

Tibes is located within the SIP, about six miles north of the city of Ponce (Figure 4). It is accessible along the Río Portugués, which has exposed the host rocks and at least 16 massive magnetite ore bodies (Figure 6; Giovannetti-Nazario & Hudgins, 2019). The ore bodies are subparallel in orientation and range between two and 10 feet in width. Many of the magnetite bodies have sharp linear contacts with the surrounding host rock (Figure 6) while others have less clearly defined contacts and a higher abundance of garnet (Figure 7). The linear magnetite bodies have an orientation of ~15°NW and are roughly parallel to local faulting identified by Krushensky & Monroe (1978). Both vein-like and disseminated calcite, epidote, garnet, and hematite are present throughout the deposit. Pyrite and chalcopyrite are not abundant but are

Figure 6. Field photo showing two linear magnetite bodies at the Tibes deposit exposed along the Rio Portugués (seen on the left). These bodies are roughly parallel and composed of ≥80% magnetite. White scale card = six inches. Photo provided by Dr. Thomas Hudgins.

present. The diorite stock outcrops along the Rio Portugués at the southern end of the deposit but is difficult to access due to vegetation and segments of river with deep water.

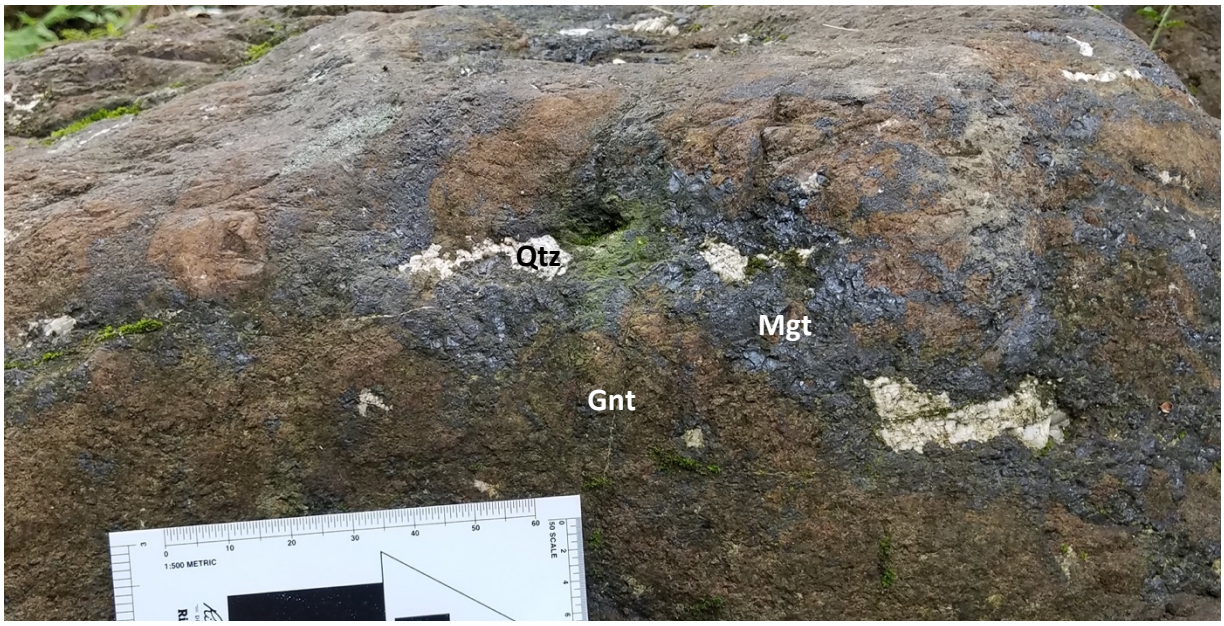

Figure 7. Field photo of magnetite with weakly defined contacts, abundant garnet, and pockets of quartz. Photo provided by David Giovannetti-Nazario.

7. Sample Collection

Samples were obtained during two field excursions: in 2020, Dr. Tom Hudgins and students David Giovannetti-Nazario and Gabriel Torres-Matos (University of Puerto Rico, Mayagüez; UPRM) collected five samples from the ore bodies of Tibes; in 2021, the Auburn team joined them to collect ten additional ore samples. The goal of sample collection was to collect spatially constrained samples both across the deposit and within individual magnetite bodies. This strategy was informed by initial trace element analysis of three samples from 2020 field work that revealed variations within and between magnetite grains.

A Shaw backpack core drill with a 41 mm barrel diameter was used to ensure extraction of the freshest magnetite possible (Figure 8A). A total of 17 samples were collected, including

15 magnetite samples, one diorite sample, and one sample of a dike adjacent to ore body #7. All samples were collected along the Rio Portugués, and their locations are shown in Figure 9. Twelve of the 15 magnetite samples were drilled, and these core samples encompass eight individual magnetite bodies across the deposit. Linear ore bodies exhibited an approximately parallel trend of ~15°NW. All core samples were split in half lengthwise; the UPRM members of the team kept one half, and the other was taken back to Auburn University (Figure 8B). Samples Sk.2ab, 21TS-MB05, 21TS-MB06, and 21TS-MB07 were taken from the same magnetite body (ore body #4) to investigate potential intra-body variation (Figure 10).

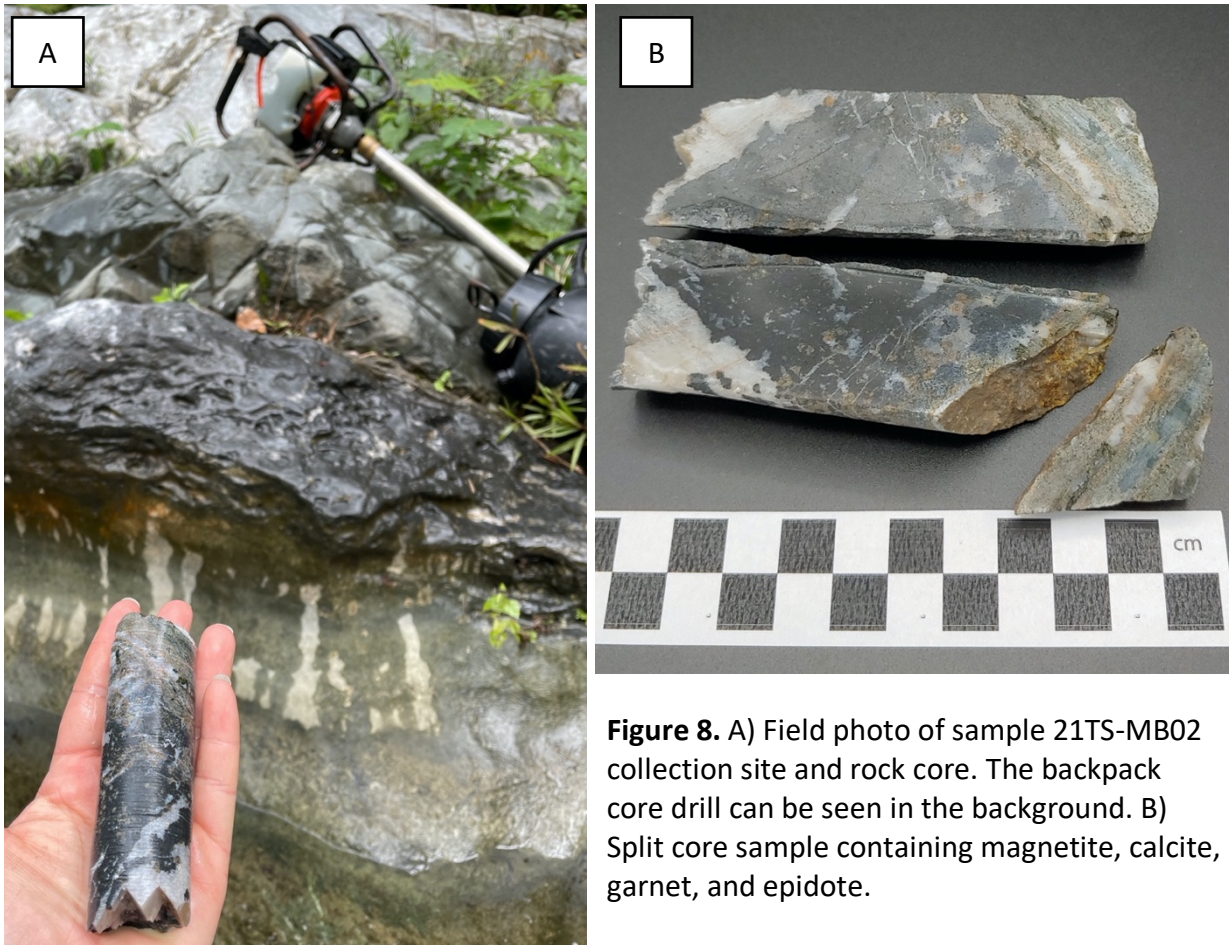

Figure 8. A) Field photo of sample 21TS-MB02 collection site and rock core. The backpack core drill can be seen in the background. B) Split core sample containing magnetite, calcite, garnet, and epidote.

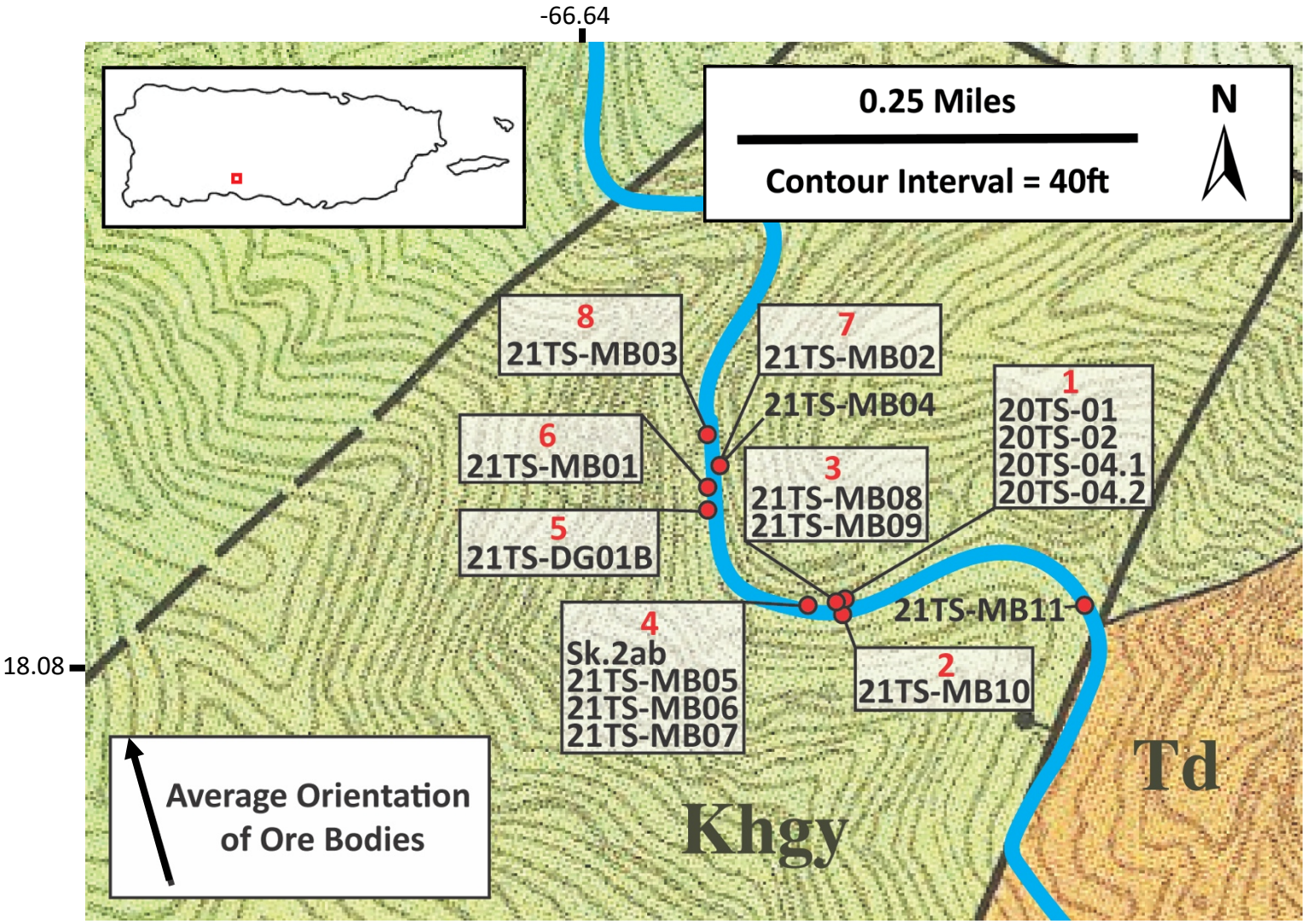

Figure 9. Locations of Tibes samples identified on a geologic map of the area. Sample descriptions and coordinates are provided in Appendix A. The blue line represents the Rio Portugués. Khgy = Hornfelsed Lago Garzas and Yauco Formations. Td = Hornblende-Augite Diorite and Quartz Diorite. Qa = Alluvium (modified from Krushensky & Monroe, 1978).

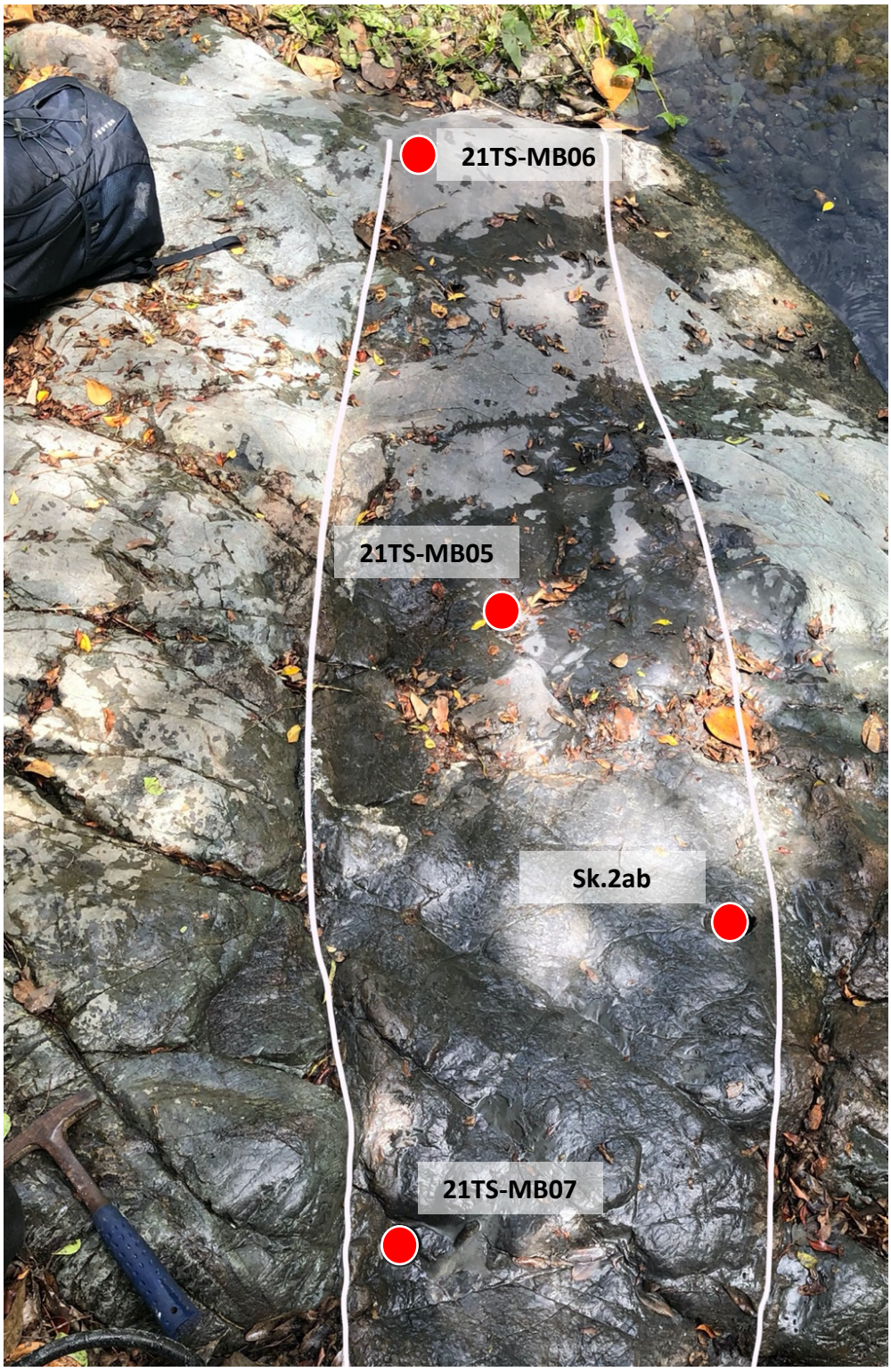

Figure 10. Drill core sampling locations across magnetite ore body #4 at the Tibes iron deposit. Extent of body outlined with a white line. Rock is wet and partially covered with debris. A rock hammer is pictured in the bottom left for scale.

8. Analytical Methodology

8a. Petrography

Petrographic observations were performed using a Nikon Eclipse Ci-POL microscope paired with the Nikon DS-Ri camera in the Auburn University Department of Geosciences. Opaque mineral phases such as magnetite and pyrite were observed using reflected light (RL) and transmitted light (plane-polarized light, PPL and cross-polarized light; XPL) was used to observe minerals such as hematite, sericite, calcite, and serpentine. These techniques allowed for characterization of mineralogy, mineral textures, and compositional zoning.

8b. Trace Element Analysis

Three samples from Dr. Thomas Hudgins's 2020 field work were sent to Spectrum Petrographics, Inc. where microprobe quality thin sections were prepared. Samples collected during 2021 field work were prepared as epoxy round mounts. To make these mounts, characteristic rock chips (3-5) for each sample were set in epoxy and polished using a series of silicon carbide sandpapers followed by 1 μm alumina powder. Two complementary methods were used to analyze the trace element composition of Tibes magnetite ore: Electron microprobe analysis (EMPA) and laser ablation inductively coupled plasma mass spectrometry (LA-ICP-MS). EMPA was conducted with a JEOL JXA-8600 electron microprobe equipped with four wavelength dispersive spectrometers at the Auburn University Electron Microprobe Analysis Lab (AU-EMPA). All samples were carbon coated prior to EMPA.

In addition to analyzing representative magnetite grains from each sample, magnetite that was identified petrographically to be zoned were imaged using backscattered electrons (BSE) to qualitatively characterize compositional zoning. Zoned magnetite was analyzed with

wavelength dispersive spectrometry (WDS) to quantitatively characterize the zoning of trace elements across grains. The beam conditions for WDS point and line analyses were 20 kV and 20 nA. Magnetite standard 114887 from the National Museum of Natural History was analyzed at the beginning and end of each session. WDS was also used to create elemental maps of zoned grains using the following conditions: 15 kV, 50 nA, 0.3 μm pixel size, and 60 second dwell time. False color was applied to WDS maps using the ImageJ software. Energy dispersive spectrometry (EDS) was used to qualitatively identify the composition of secondary minerals found within veins and vugs. The complete EMPA data set is included in Appendix B. EMPA conditions, quantification setup, and standardization information are summarized in Table 1. No correction was applied for Ti-V interferences.

Table 1. EMPA conditions, quantification setup, and standardization at Auburn University using a JEOL JXA-8600

Element	Crystal	Standard	Reference Name	Formula
Na	TAP	Albite	Amelia	Na_2O
Mg	TAP	Olivine	Ol 2566	MgO
Al	TAP	Anorthite	Great Sitkin	Al_2O_3
Si	TAP	Wollastonite	-	SiO_2
Ca	PET	Wollastonite	-	CaO
Ti	PET	Ilmenite	-	TiO_2
Cr	PET	Chromite	-	Cr_2O_3
Fe	LIF	Magnetite	USNM 114887	Fe_3O_4
Mn	LIF	Garnet	P-130	MnO

The trace element composition of magnetite was also determined using a NWR193 193nm Excimer laser ablation (LA) system coupled to an Agilent 7900 inductively coupled plasma mass spectrometer (ICP-MS) at Auburn University. The main advantages of laser ablation inductively coupled plasma mass spectrometry (LA-ICP-MS) are that it has a lower detection limit than EMPA for many elements and it is possible to run an analysis of the entire

suite of trace elements at once. Synthetic glass NIST 610 (National Institute for Standards and Technology) and natural basalt glass BCR-2GA (Columbia River Basalt from the United States Geological Survey) were used as reference materials and were analyzed several times throughout each run to monitor for instrumental drift. Oxide ratios were monitored before the start of each analysis. ^{57}Fe was used as an internal standard based on EMPA values for Tibes magnetite. Pre-ablation passes were performed on some samples to smooth out irregular surfaces. Laser conditions are summarized in Table 2. All data were processed with the iolite v.4 software.

Table 2. LA-ICP-MS conditions at Auburn University

Laser ablation system	Excimer NWR193
ICP-MS	Agilent 7900 ICP-MS
Analyzed isotopes	^{24}Mg, ^{25}Mg, ^{27}Al, ^{29}Si,^{43}Ca, ^{44}Ca, ^{47}Ti, ^{49}Ti, ^{51}V, ^{52}Cr, ^{53}Cr, ^{55}Mn, ^{56}Fe, ^{57}Fe, ^{59}Co, ^{60}Ni, ^{71}Ga
Magnetite	
Laser frequency	16 Hz
Stage speed	2 μm/s
Beam size	30 μm
Laser power	~3.4 J/cm^2
Standards	
Laser frequency	16Hz
Stage speed	5 μm/s
Beam size	30 μm
Laser power	~3.4 J/cm^2
Pre-ablation Conditions	
Laser frequency	5 Hz
Beam size	60 μm
Laser power	~1.8 J/ cm^2
Internal standard	^{57}Fe (values from EMPA)
Reference material	NIST 610 (synthetic glass) BCR-2GA (natural glass)
Data processing	iolite v.4

8c. Stable Isotope Geochemistry

The iron isotope composition of Tibes magnetite was determined by collaborators at the University of British Columbia (UBC) using a Nu Plasma 1700 (Nu Instruments, Wrexham, UK) multi-collector inductively coupled mass spectrometer (MC-ICP-MS) in the Pacific Centre for Isotopic and Geochemical Research (PCIGR). This model of MC-ICP-MS allows for the complete removal of isobaric interferences from iron signals due to its large geometry and special detector design. This is important because differences in iron isotope abundances can be very small; most MC-ICP-MS instruments only partially separate interfering signals, which affects the accuracy and precision of measurements. Magnetite samples (~2mg) were first separated at Auburn University, crushed to a fine powder, then dissolved completely at UBC at 120°C in capped Savillex vials, first in concentrated HNO_3 + HF then with HCl. The iron was subsequently isolated via ion chromatography following the procedure of Bilenker et al. (2018) using BioRad AG MP-1M 100-200 mesh resin. The resulting iron was dried down, twice dissolved in ~500µl of 2% HNO_3 and dried down to further purify the solution before being dissolved in 10ml of 2% HNO_3 and introduced into the MC-ICP-MS in dry plasma mode using a DSN-100. All chemical sample preparation was performed in PCIGR clean laboratories, which house class 100 fume hoods within a class 1000 clean room.

Standard 14 from the Institute for Reference Materials and Measurements (IRMM-14) was also dissolved in 2% HNO_3 and analyzed between each sample to monitor and correct for instrumental drift by standard-sample bracketing. Reference materials BCR-2 and BHVO-2 from the U.S. Geological Survey were processed and analyzed following the same procedures as the samples to monitor for accuracy throughout the session. All standards, reference materials, and

samples were diluted to have iron concentrations that matched within 10%. Chromium corrections were made online to ^{54}Fe measurements by monitoring ^{52}Cr. All adjustments were negligible.

For oxygen isotope analysis, magnetite samples (~2mg) were sent to Dr. Ilya Bindeman at the Stable Isotope Laboratory in the Department of Earth Sciences at the University of Oregon. Samples were analyzed using a laser fluorination line, with BrF_5 as the reagent, attached to a MAT 253 gas isotope ratio mass spectrometer (IRMS). This technique is faster than the traditional method of using furnaces to release oxygen from the sample, allows for much smaller sample sizes, and reduces instrumental isotope fractionation. Gore Mountain Garnet was used as the standard and analyzed at the beginning and end of each set of analyses. Some magnetite samples had to be pre-fluorinated to remove any adsorbed water and achieve an acceptable blank.

9. Results

9a. Petrography

Samples of the Tibes iron ore are composed of ~80% magnetite, and the remaining 20% is a combination of secondary minerals including sericite, serpentine, hematite, calcite, pyrite, and chalcopyrite (Figure 11). Petrographic observations of magnetite and secondary minerals are summarized in Table 3. Some magnetite is euhedral, while other parts are more massive, which makes it hard to identify grain boundaries (Figure 11). Between magnetite grains there are large (up to 0.1 cm in diameter) vugs containing other minerals. Within magnetite grains, there are smaller scale voids (5 to 50 μm) that sometimes contain minerals but are often empty (Figure 11C, D, and E). Many magnetite grains are zoned with micro-inclusions that are only

visible with at least 50x magnification (Figure 11D). Simple zoning is common in smaller magnetite grains, while many larger grains exhibit oscillatory zoning, with a distinct core and rim, which is common in hydrothermal deposits (Dare et el., 2014). Several of these zoned grains were imaged and targeted for EMPA. Smaller grains have more simple zoning.

Secondary minerals occur in vugs and veins throughout the samples (Table 3; Figure 11). Veins are most often rich in calcite and/or hematite with minor sericite, serpentine, pyrite, and chalcopyrite, while vugs are often filled with a mixture of sericite, calcite, serpentine, and hematite with minor pyrite and lesser chalcopyrite. Pyrite occurs as both anhedral and cubic crystals (Figure 12). Euhedral pyrite grains are rare within the ore bodies and only occur within large calcite veins. Anhedral, smaller pyrite grains are common within vugs and are associated with either calcite or silicate minerals. Fractures through and around magnetite grains often contain secondary hematite.

Table 3. Summary of petrographic observations of the Tibes samples.

Magnetite	Veins	Vugs
• **Vugs** and **fractures** within and between grains • Some **euhedral**, some massive • Most zoned, some **oscillatory zoning**	• Rich in **calcite** and **hematite** +/- **sericite** and **serpentine** • Minor **pyrite** with lesser **chalcopyrite**	• **Sericite**, **calcite**, and **hematite** • Minor **pyrite** with lesser **chalcopyrite**

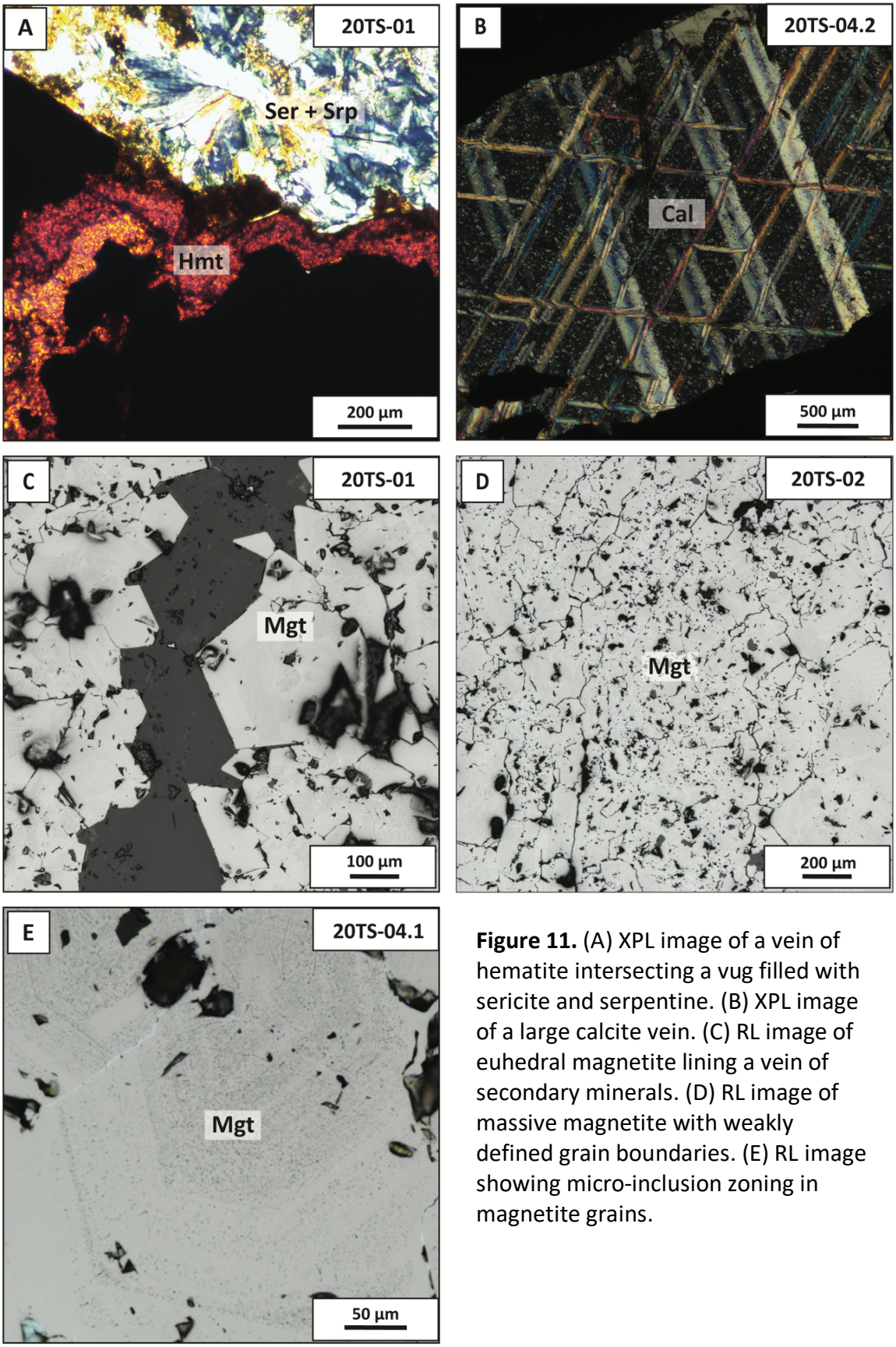

Figure 11. (A) XPL image of a vein of hematite intersecting a vug filled with sericite and serpentine. (B) XPL image of a large calcite vein. (C) RL image of euhedral magnetite lining a vein of secondary minerals. (D) RL image of massive magnetite with weakly defined grain boundaries. (E) RL image showing micro-inclusion zoning in magnetite grains.

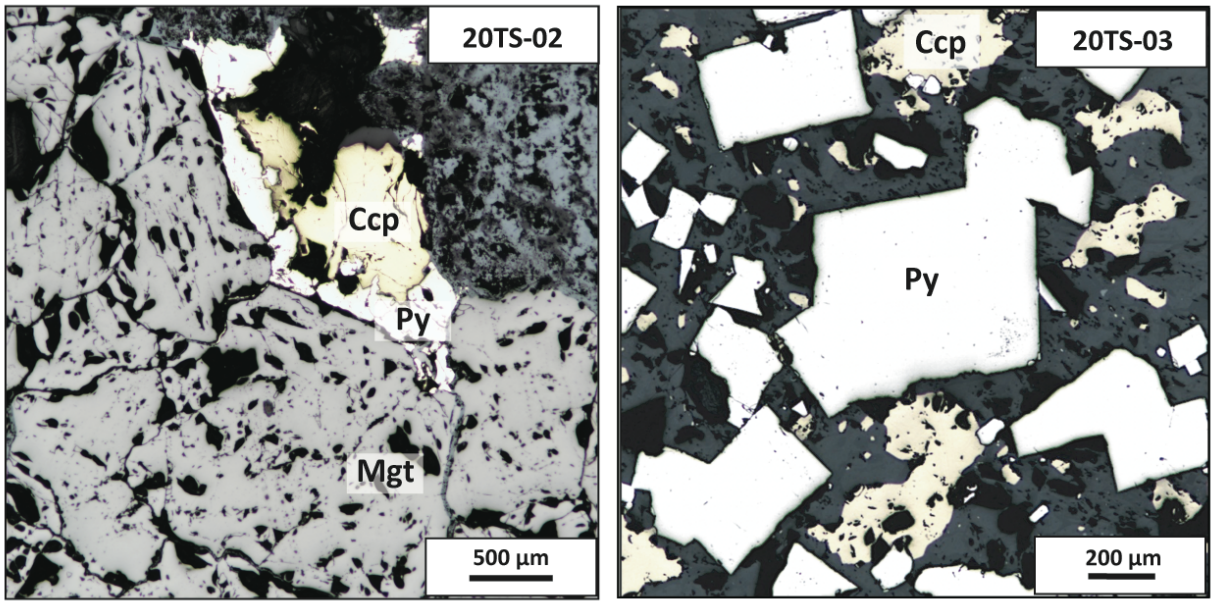

Figure 12. (Left) RL image of sulfides within a vug filled with sericite and serpentine. Pyrite can be seen partially filling in the space between magnetite grains. (Right) Cubic pyrite with chalcopyrite within a large (~0.5 cm) calcite vein.

9b. Magnetite Zonation

BSE imaging of Tibes magnetite revealed compositional zoning consistent with the zoning of micro-inclusions identified via petrographic microscopy (Figure 13). The zoned magnetite in the center of Figure 13 was targeted for WDS analysis of dark and light bands. Dark bands correspond to zones wither lower average atomic number, and these contain higher concentrations of Si and Ca and lower concentrations of Fe in comparison to light bands within the same grain. Average concentrations of these elements for dark and light bands are summarized in Table 4.

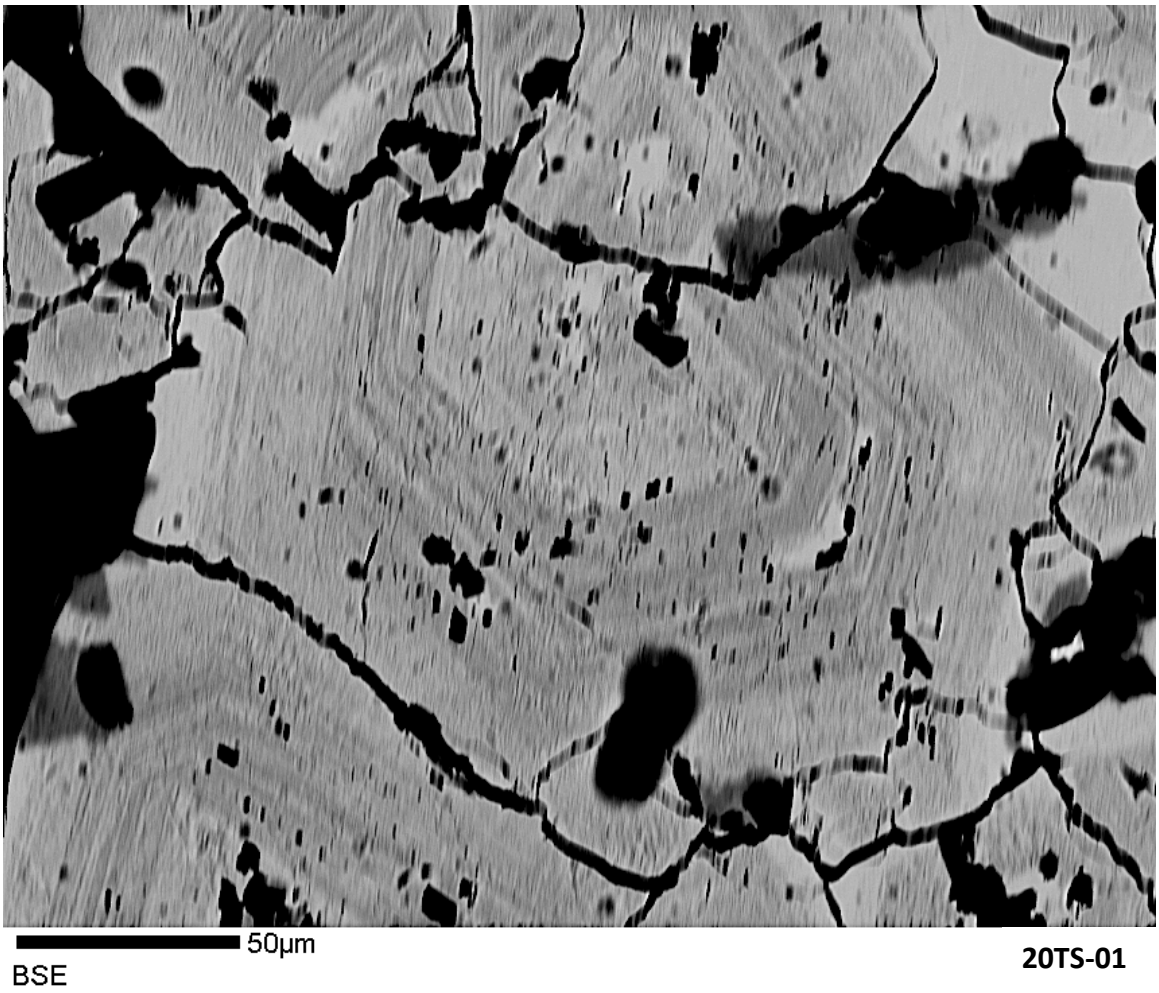

Figure 13. BSE image of zoned magnetite grains in sample 20TS-01. Zoning is oscillatory and distinct cores and rims can be identified. Image obtained in the Auburn University Electron Microprobe Analysis Lab (AU-EMPA).

Table 4. Average concentrations for Si, Ca, and Fe in dark and light bands seen in the BSE image in Figure 13. The full data set is included in Appendix B. Z = average atomic number.

	Si (wt%)	Ca (wt%)	Fe (wt%)
Light (n=6), Higher Z	0.60	0.22	70.65
Dark (n=5), Lower Z	1.73	0.70	68.38

A second zoned magnetite grain was mapped with WDS, which also showed increased Si and Ca within darker bands (Figure 14). No other systematic zoning was identified by WDS maps. All EMPA data is included in Appendix B.

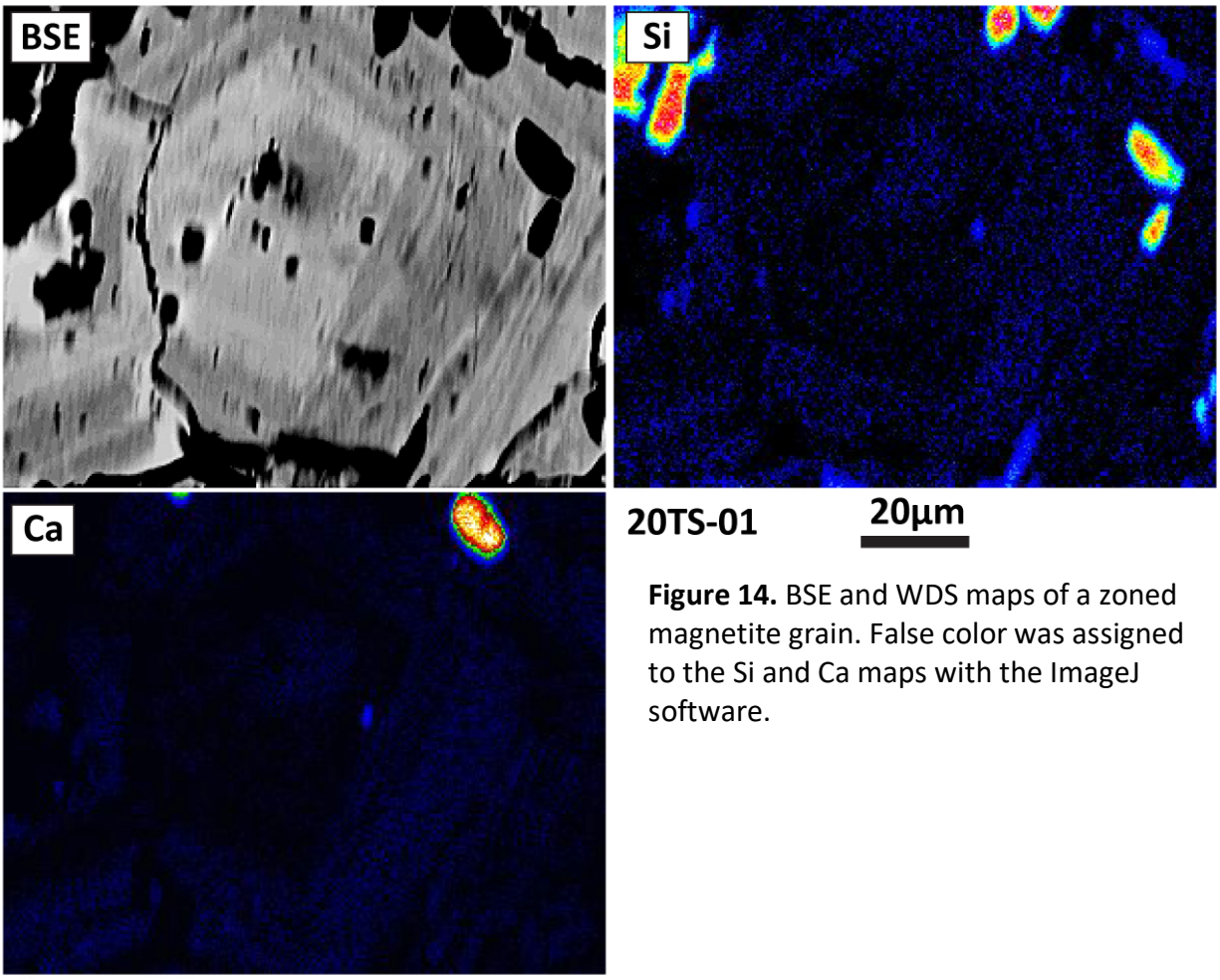

Figure 14. BSE and WDS maps of a zoned magnetite grain. False color was assigned to the Si and Ca maps with the ImageJ software.

9c. Trace Element Concentrations in Tibes Magnetite

Average trace element concentrations obtained by LA-ICP-MS for Tibes magnetite are reported in Table 5 below. The complete data set, including 2σ errors, is included in Appendix C. A total of 14 samples from eight ore bodies were analyzed. ThO/Th ratios were between 0.163% and 0.204% over five days of analysis.

Table 5. Trace element and Fe concentrations (wt%) for Tibes magnetite determined using LA-ICP-MS. Prefixes "20TS" and "21TS" have been removed from the sample names. Bold sample names indicate that the sample was pre-ablated.

	02	04.1	04.2	**MB10**	**MB08**	**MB09**	Sk.2ab
Ore Body #	1	1	1	2	3	3	4
^{27}Al	0.21	0.21	0.20	0.12	0.45	0.18	0.25
^{29}Si	1.79	1.41	1.13	0.47	1.07	0.42	0.76
^{43}Ca	0.52	0.44	0.33	0.15	0.44	0.20	0.26
^{44}Ca	0.49	0.42	0.34	0.15	0.45	0.20	0.25
^{47}Ti	0.03	0.04	0.03	0.05	0.04	0.02	0.03
^{49}Ti	0.03	0.05	0.03	0.05	0.03	0.02	0.03
^{51}V	0.00	0.00	0.00	0.00	0.00	0.00	0.00
^{52}Cr	0.00	0.00	0.00	0.00	0.00	0.00	0.00
^{53}Cr	0.00	0.00	0.00	0.00	0.00	0.00	0.00
^{55}Mn	0.10	0.10	0.10	0.07	0.13	0.06	0.13
^{56}Fe	72.82	73.20	69.56	69.88	66.69	73.47	70.24
^{59}Co	0.00	0.00	0.00	0.00	0.00	0.00	0.00
^{60}Ni	0.00	0.00	0.00	0.00	0.00	0.00	0.00
^{71}Ga	0.00	0.00	0.00	0.00	0.00	0.00	0.00
Ti+V	0.03	0.05	0.04	0.05	0.04	0.02	0.03
Ca+Al+Mn	0.83	0.74	0.62	0.35	1.02	0.44	0.64
n	7	6	6	5	6	4	5

Table 5 (continued). Trace element and Fe concentrations (wt%) for Tibes magnetite determined using LA-ICP-MS. Prefixes "20TS" and "21TS" have been removed from the sample names. Bold sample names indicate that the sample was pre-ablated.

	MB05	**MB06**	MB07	DG01B	MB01	MB02	**MB03**
Ore Body #	4	4	4	5	6	7	8
^{27}Al	0.15	0.38	0.26	0.13	0.23	0.31	0.18
^{29}Si	0.50	0.76	0.53	0.17	0.87	1.13	0.41
^{43}Ca	0.20	0.31	0.17	0.02	0.23	0.35	0.10
^{44}Ca	0.20	0.31	0.17	0.02	0.22	0.33	0.09
^{47}Ti	0.04	0.02	0.07	0.01	0.02	0.02	0.01
^{49}Ti	0.04	0.02	0.07	0.01	0.02	0.02	0.01
^{51}V	0.00	0.00	0.01	0.00	0.00	0.00	0.00
^{52}Cr	0.00	0.00	0.00	0.00	0.00	0.00	0.00
^{53}Cr	0.00	0.00	0.00	0.00	0.00	0.00	0.00
^{55}Mn	0.07	0.11	0.05	0.07	0.08	0.10	0.09
^{56}Fe	73.34	68.83	67.69	71.99	70.96	71.20	69.55
^{59}Co	0.00	0.00	0.00	0.00	0.00	0.00	0.00
^{60}Ni	0.00	0.00	0.00	0.00	0.00	0.00	0.00
^{71}Ga	0.00	0.00	0.00	0.00	0.00	0.00	0.00
Ti+V	0.04	0.03	0.08	0.01	0.02	0.02	0.01
Ca+Al+Mn	0.42	0.80	0.48	0.22	0.54	0.76	0.37
n	5	5	3	6	5	3	6

9d. Stable Fe and O Isotope Compositions of Tibes Magnetite

Oxygen and Fe isotope compositions of Tibes magnetite are reported in Table 6. Oxygen isotope values are reported in delta notation relative to Vienna-Standard Mean Ocean Water (VSMOW) following Equation 1:

$$\delta^{18}O = \left[\frac{\left({}^{18}O/_{16}O \right)_{Sample}}{\left({}^{18}O/_{16}O \right)_{VSMOW}} - 1 \right] \text{x } 1000 \qquad (1)$$

$\delta^{18}O$ values for Tibes magnetite (15 samples from eight ore bodies) are between 2.83‰ to 5.02‰. Analyses of the Gore Mountain Garnet standard resulted in $\delta^{18}O \pm 2\sigma$ values of 6.52 $\pm$ 0.07‰, 6.52 $\pm$ 0.07‰, and 6.43 $\pm$ 0.33‰, over three days of analyses.

Iron isotope compositions of Tibes magnetite are reported in delta notation relative to IRMM-14 following Equation 2:

$$\delta^{56}Fe = \left[\frac{\left({}^{56}Fe/_{54}Fe \right)_{Sample}}{\left({}^{56}Fe/_{54}Fe \right)_{IRMM-14}} - 1 \right] \text{x } 1000 \qquad (2)$$

$\delta^{56}Fe$ compositions of Tibes magnetite are between 0.13‰ to 0.39‰. Analyses of BCR-2 resulted in $\delta^{56}Fe \pm 2\sigma$ values of 0.09 $\pm$ 0.05‰ (n=2) and 0.10 $\pm$ 0.04‰ (n=4) over two days; the accepted value is 0.09‰ (Craddock & Dauphas, 2011). Analyses of BHVO-2 resulted in $\delta^{56}Fe \pm 2\sigma$ values of 0.12 ± 0.05‰ (n=3), 0.10 $\pm$ 0.04‰ (n=3), and 0.13 $\pm$ 0.05‰ (n=2), respectively over three days; the value accepted in the literature is 0.11‰ (Craddock & Dauphas, 2011).

Table 6. Isotope compositions of Tibes magnetite. Dashes indicate missing duplicate value.

Sample #	Magnetite Body	$\delta^{18}O$	$\pm 2\sigma$	$\delta^{56}Fe$	$\pm 2\sigma$	n
Sk.0*	-	4.36	0.07	0.21	0.03	3
		-	-	0.26	0.08	3
Sk.2ab	4	3.35	0.07	0.39	0.01	3
20TS-01	1	3.92	0.07	0.24	0.02	3
20TS-02	1	3.46	0.07	0.28	0.06	3
20TS-04**	1	4.80	0.07	0.23	0.05	3
		-	-	0.23	0.09	2
21TS-MB01	6	3.03	0.33	0.23	0.02	3
21TS-MB02	7	2.83	0.33	0.20	0.02	3
21TS-MB03*	8	3.70	0.33	0.19	0.03	3
		-	-	0.17	0.03	3
21TS-MB05**	4	4.75	0.33	0.20	0.04	3
	4	-	-	0.26	0.05	3
21TS-MB06	4	5.02	0.33	0.19	0.03	3
21TS-MB07	4	4.20	0.33	0.25	0.03	3
21TS-MB08*	3	3.40	0.33	0.13	0.03	4
	3	-	-	0.16	0.02	3
21TS-MB09	3	3.62	0.33	0.19	0.02	3
21TS-MB10	2	4.27	0.33	0.22	0.01	3
21TS-DG01B**	5	3.45	0.33	0.15	0.04	3
		-	-	0.19	0.04	4

*Duplicates were analyzed for Fe but not for O. **Replicates were analyzed for Fe.

10. Discussion of Results

10a. Skarn Characterization based on Trace Element Variations

The variation of trace elements between magmatic and hydrothermal magnetite is well documented and can be used to determine the environment in which ore magnetite formed (Dare et al., 2014; Knipping et al., 2015b). Discrimination plots developed by Dupuis and Beaudoin (2011), refined by Dare et al. (2014) and Nadoll et al. (2015) allow for the determination of deposit type based on iron oxide trace element compositions (Figure 15).

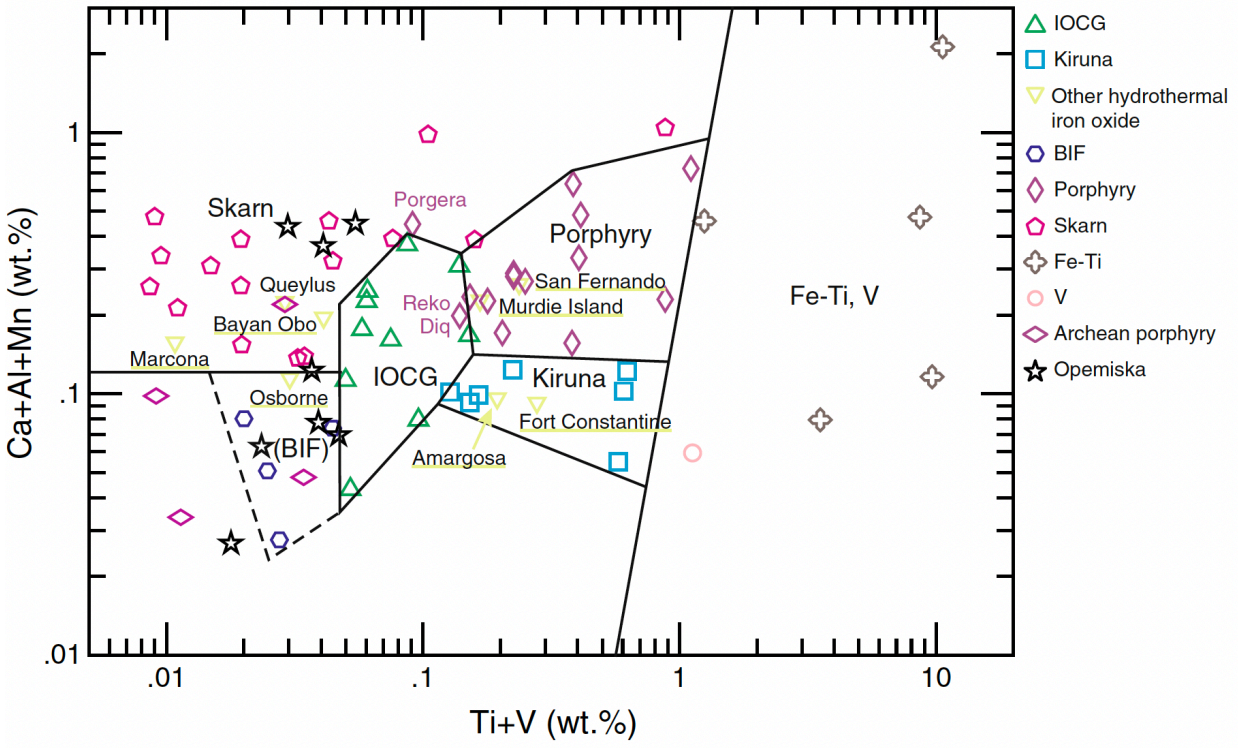

Figure 15. Discrimination diagram from Dupuis & Beaudoin (2011) that allows for the determination of deposit type based on iron oxide composition. Discriminatory bins were determined based on iron oxide data from iron oxide copper-gold (IOCG), Kiruna/iron oxide-apatite (IOA), banded iron formation (BIF), porphyry copper, skarn, and Fe-Ti-V deposits.

Importantly, since mineral inclusions have been identified in both igneous and hydrothermal magnetite (e.g., Dare el al., 2014; Huang & Beaudoin, 2021; Nadoll et al., 2014) great care needs to be taken when analyzing and interpreting trace element compositions of magnetite; discriminatory fields must be used with caution.

Elements that are relatively fluid-immobile, such as Ti and Al, tend to be enriched in magnetite from magmatic systems, while elements such as Si and Ca tend to be enriched in hydrothermal magnetite (Dare et al., 2014). The variable behavior of these elements is reliant on multiple factors such as temperature, pH, compatibility, and redox. Since these behaviors are well characterized by field-based studies (e.g., Dare et al., 2014; Nadoll et al., 2015; Duran et al., 2020) and petrologic experiments (e.g., Lindsley, 1991), we can use the measured concentrations of these elements to understand the formation and history of these deposits (e.g. Dupuis & Beaudoin, 2011, Dare et al., 2014; Nadoll et al., 2015; Duran et al., 2020).

The average concentrations of key mobile (V, Ca, Mn) and immobile (Ti and Al) trace elements in Tibes magnetite are summarized in Figure 16. Overall, concentrations of Ti, V, Ca, Al, and Mn are consistent with magnetite from other skarn deposits, and variations in trace element composition can be observed across the deposit, within ore bodies, and within individual samples. All Tibes magnetite has very low concentrations of the elements Ti and Cr, which both complicate ore processing. Samples that are proximal to the diorite stock are relatively enriched in Ti, V, Ca, Al, and Mn, and those more distal are relatively depleted in the same elements (Figure 16). This is likely due the fact that magnetite higher concentrations of these elements at higher temperatures and in magmatic systems.

Variations between ore bodies and on a deposit-wide spatial scale (tens of meters), highlight the importance of strategic and extensive sampling. It also implies that with intentional, detailed sampling, one may be able to vector toward the source pluton of a skarn based on variations in magnetite trace element geochemistry. This could also potentially locate a porphyry deposit since the source plutons of skarns are often also associated with porphyries.

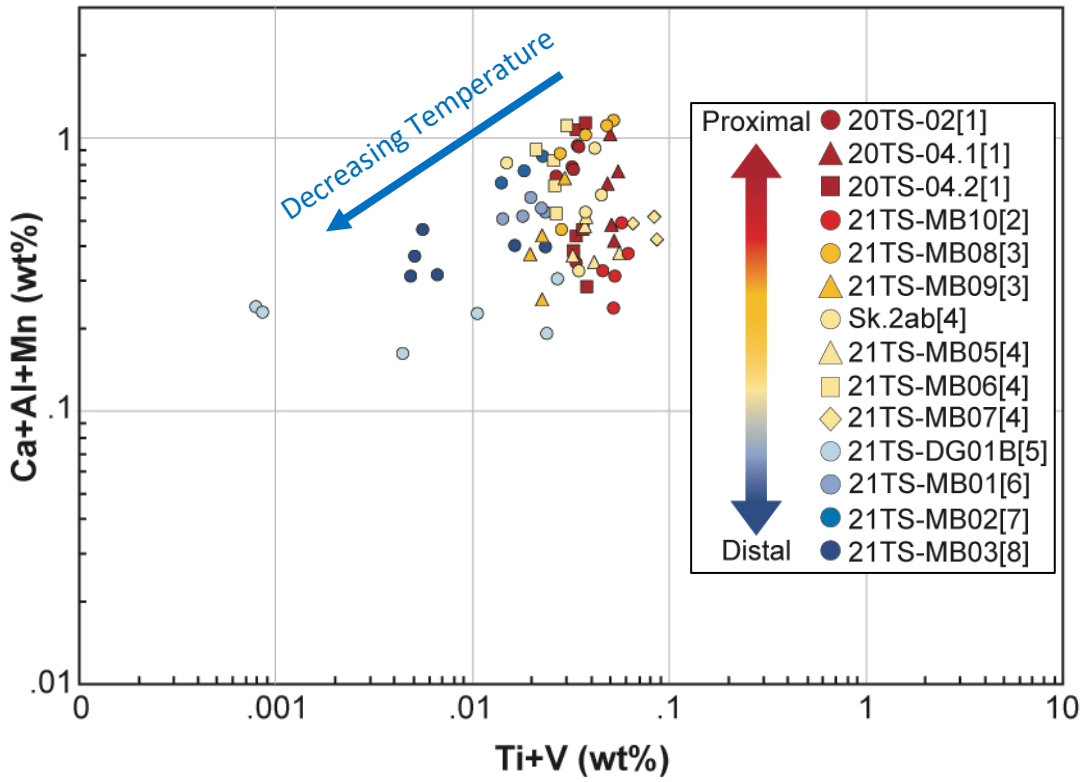

Figure 16. Trace element compositions (Ti+V vs. Ca+Al+Mn) of Tibes magnetite determined by LA-ICP-MS. Samples from the same ore body are plotted in the same color and individual samples are given their own shape. The ore body number is within brackets at the end of the sample name. The color of the data point also indicates its proximity to the diorite stock, with dark red being most proximal and dark blue being most distal.

It should be noted that the presence of micron-scale inclusions within Tibes magnetite grains does complicate the interpretation of magnetite trace element data, as mentioned in section 9b. Analyses contaminated by micron-scale mineral inclusions present within oscillatory zones are expected to have higher concentrations of Si and Ca, and lower concentrations of Ti and V in comparison to coeval magnetite (Figure 16). Elemental measurements by EMPA of zonation identified in BSE imaging (Figure 13) confirmed increased concentrations of Si and Ca in darker bands relative to lighter bands (Figure 17). Silicon and Ca are incompatible in magnetite (Nadoll et al., 2014 and references therein), so the enrichment of these elements indicates an increased abundance of silicate inclusions.

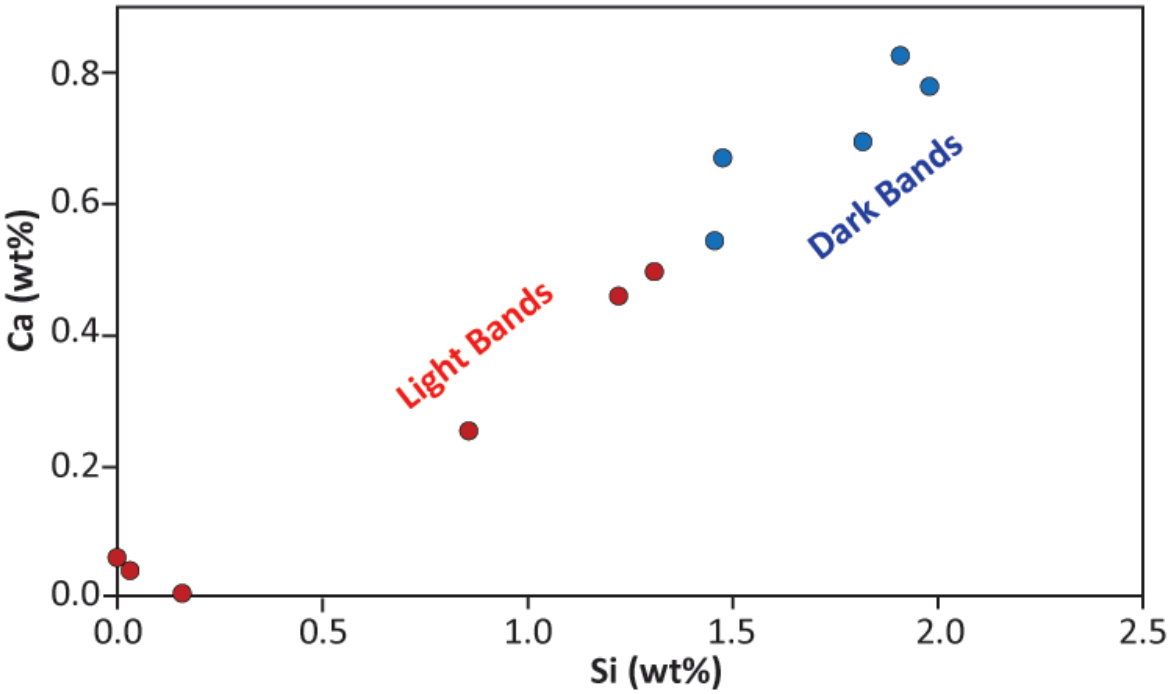

Figure 17. EMPA data (Si vs Ca) for dark and light bands present in three zoned magnetite grains identified in the BSE image in Figure 13. The full data for these analyses are in Appendix B.

10b. The Source of Fe and O in Tibes Magnetite Ore

When the O isotope composition of Tibes magnetite is evaluated alongside published magnetite $\delta^{18}O$ values from various deposit types (Figure 18), it is consistent with that of higher temperature systems like Chilean iron oxide-apatite (IOA) and iron oxide-copper-gold (IOCG) deposits, rather than that of other iron skarns. The $\delta^{18}O$ compositions of Tibes magnetite also fall well within the range of O isotope compositions defined as magmatic/high temperature (Figure 18; Taylor et al., 1967; Taylor, 1968; Bindeman, 2008). This range is indicative of magnetite that crystallized from a silicate melt or magmatic-hydrothermal fluid and is based on measurements of natural magnetite known to form in magmatic systems. Magnetite crystallized from low-temperature non-magmatic fluids exhibit notably isotopically lighter compositions than those from high-temperature systems.

The $\delta^{56}Fe$ compositions of Tibes magnetite also reflect a magmatic origin for Tibes magnetite (Figure 19) as these data are consistent with magnetite from magmatic/magmatic-hydrothermal systems like IOAs, IOCGs, porphyry deposits, and the Bushveld layered mafic intrusion. Available data for banded iron formations exhibit a wide range of $\delta^{56}Fe$ values likely because they form at low temperatures in open systems, where the magnitude of isotope fractionation is greater.

Since both the Fe and O isotope compositions of Tibes magnetite confirm a magmatic-hydrothermal origin, the diorite stock is the most likely source for the Fe and Si-rich fluids that formed the Tibes skarn ore bodies.

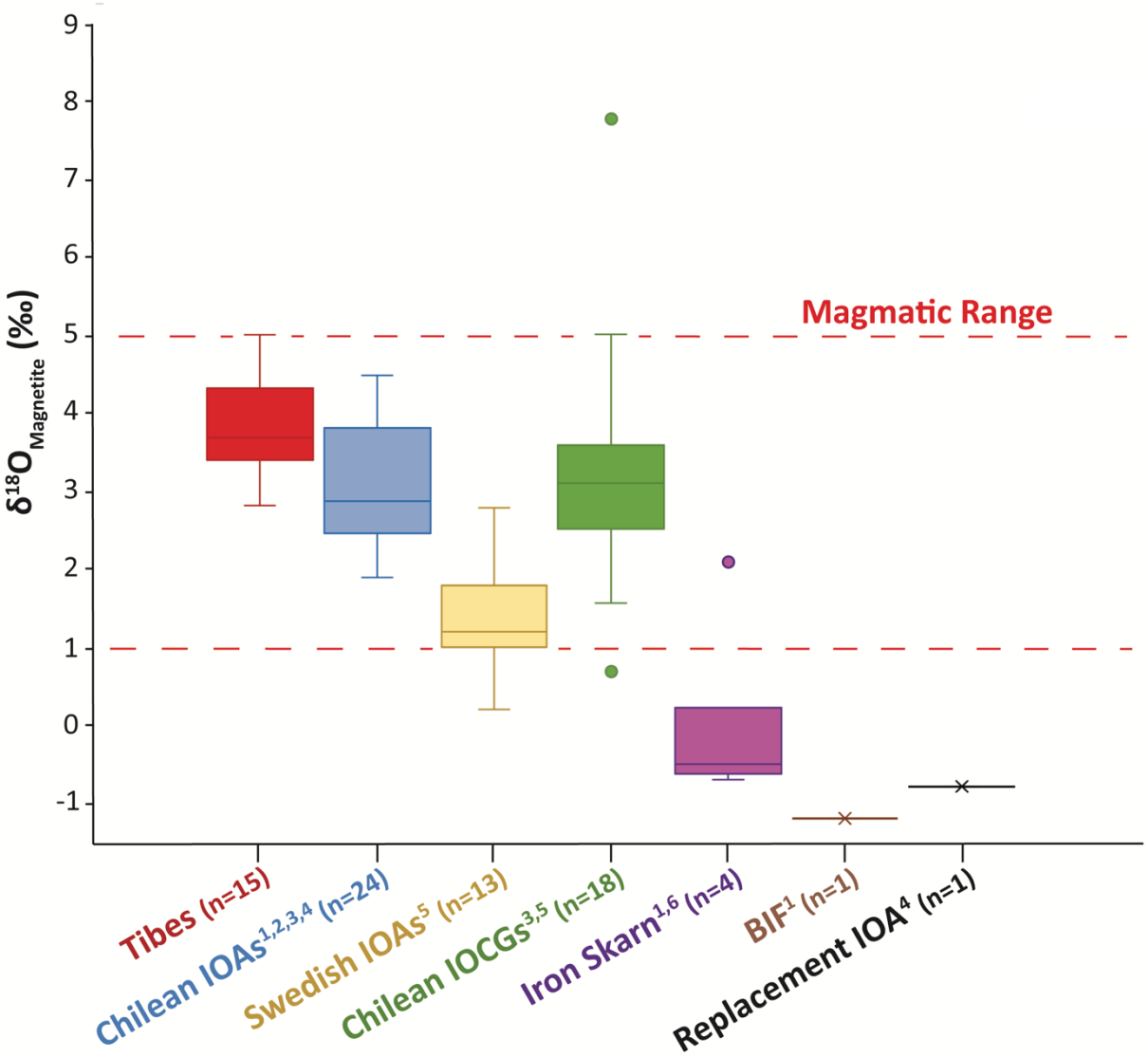

Figure18. $\delta^{18}O$ values for magnetite from various deposit types including 2σ errors. The range of magmatic values is indicated by the red dashed lines. The legend lists the deposit name followed by its location. The Mineville IOA deposit formed by hydrothermal replacement and carries a different isotopic signature than the Chilean IOAs.[1]Weis (2013); [2]Rhodes & Oreskes (1999); [3]Rodriguez-Mustafa et al. (2020); [4]Bilenker et al. (2016); [5]Childress et al. (2020); [6]Troll et al. (2019). Magmatic range defined as 1 to 5‰ by Taylor et al. (1967); Taylor (1968); Bindeman (2008).

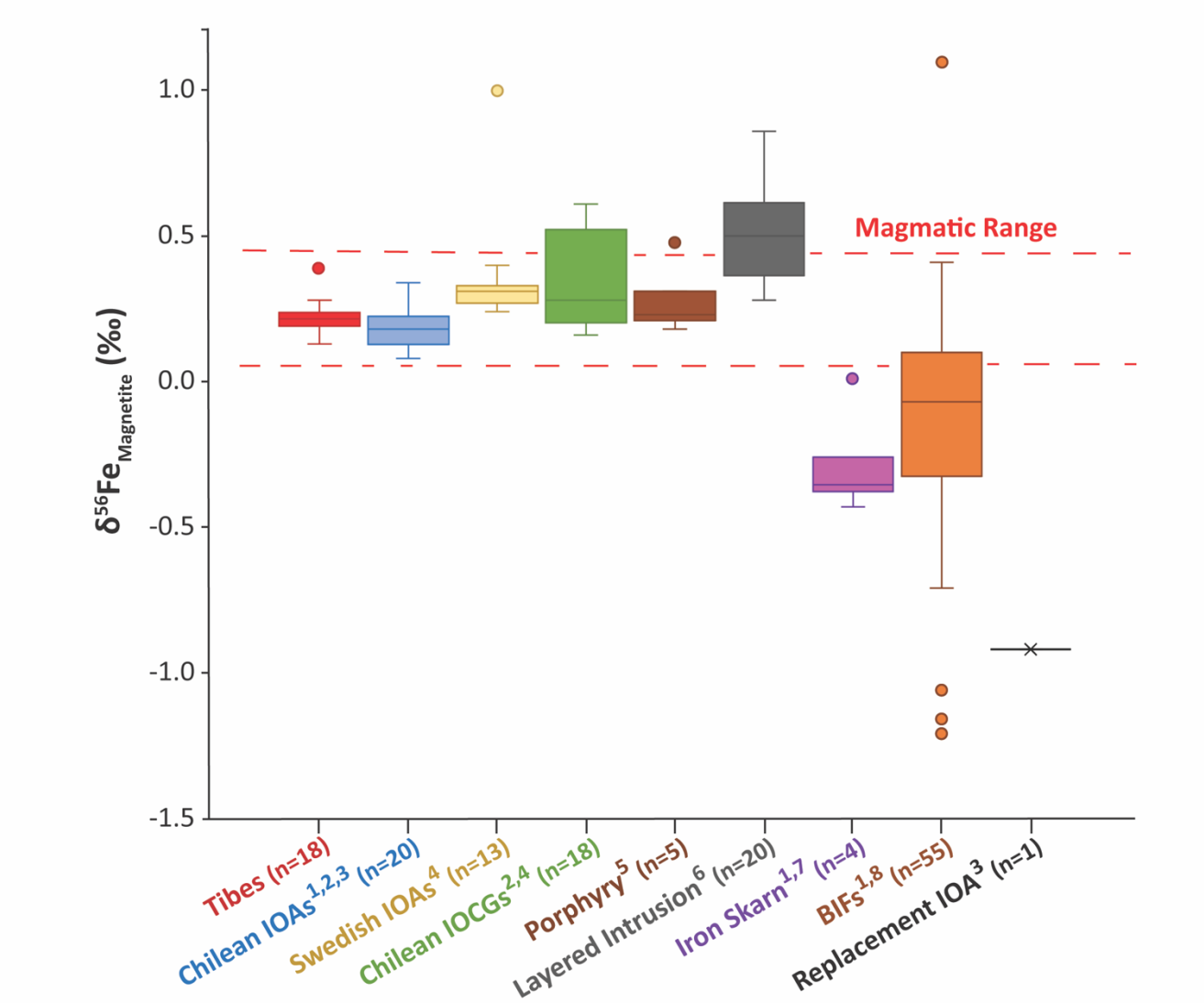

Figure 19. δ^{56}Fe compositions of magnetite from different deposit types. The magmatic range defined as 0.06 to 0.49‰ by Heimann et al. (2008) is indicated by the red dashed lines. Errors are reported as 2σ, and some error bars fall behind the data points.[1]Weis (2013); [2]Rodriguez-Mustafa et al. (2020); [3]Bilenker et al. (2016); [4]Childress et al. (2020); [5]Wawryk & Foden (2017); [6]Bilenker et al. (2017); [7]Troll et al. (2019); [8]Johnson et al. (2008).

10c. Assessing Magnetite Alteration

Pairing Fe and O isotope pairing (Fe-O) has been used widely as a method for identifying the source and alteration extent of iron oxides (e.g., Weis, 2013; Bilenker et al., 2016) and Fe-O data have been published for a range of magmatic and hydrothermal magnetite samples including those from IOCG, IOA, and porphyry deposits, two banded iron formations, and a layered mafic intrusion (Weis, 2013; Bilenker et al., 2016; Simon et al., 2019; Troll et al., 2019; Rodriguez-Mustafa et al., 2020; Childress et al., 2020). Iron-O pairs have been published for only one iron skarn so far (Weis et al., 2013; Troll et al., 2019). By comparing the isotope ratios of magnetite from the Tibes deposit to these global data from well-characterized deposits, we can determine whether the magnetite precipitated from a meteoric fluid, precipitated from an aqueous magmatic fluid (i.e., magmatic-hydrothermal origin), or crystallized from a silicate melt (i.e., magmatic origin). Additionally, post-mineralization hydrothermal alteration due to fluid/rock interactions involving meteoric water can be captured in the stable isotope signatures.

Although O isotope compositions of minerals are readily modified by post depositional alteration, this process has a minimal effect on the Fe isotope composition (Weis, 2013). This is because meteoric water contains very low concentrations of Fe in comparison to magnetite. When comparing the Fe and O isotope compositions of Tibes magnetite, it is clear that the ore is unaltered (Figure 20). This is supported by field and petrographic observations.

This is a new approach for skarns, which is why little published isotope data exists for magnetite from these deposits. Skarn systems incorporate both magmatic-hydrothermal and meteoric fluids, thus their isotopic compositions are complex records of fluid history. To fully

evaluate the application of this method to skarns, the global database must be expanded, and this study accomplishes an important first step.

10d. Comparison of Tibes Fe and O Isotopes to Other Skarn Deposits

The isotopic signatures of both Fe and O in Tibes magnetite are heavier than existing data for other iron skarns (Figure 20). One possible explanation for this is that the Tibes iron skarn is unaccreted and has not experienced extensive post depositional metamorphism. This is uncommon for calcic iron skarns as they only form in island arcs and are usually found accreted to continental margins. The intense metamorphism that takes place during the process of accretion likely alters the isotopic composition of magnetite within these skarns.

Another explanation for this discrepancy is the global data gap for isotope compositions of magnetite from iron skarns. We need more Fe isotope data from skarn magnetite to evaluate the applications of this technique to these deposits and as more data become available, other deposits may reveal heavier magnetite isotope signatures similar to Tibes.

In contrast to the trace element data, the Fe isotope composition of Tibes magnetite shows little variation between ore bodies or within individual samples. Neither Fe nor O isotope compositions show any correlation to their proximity to the diorite stock (Figure 21).

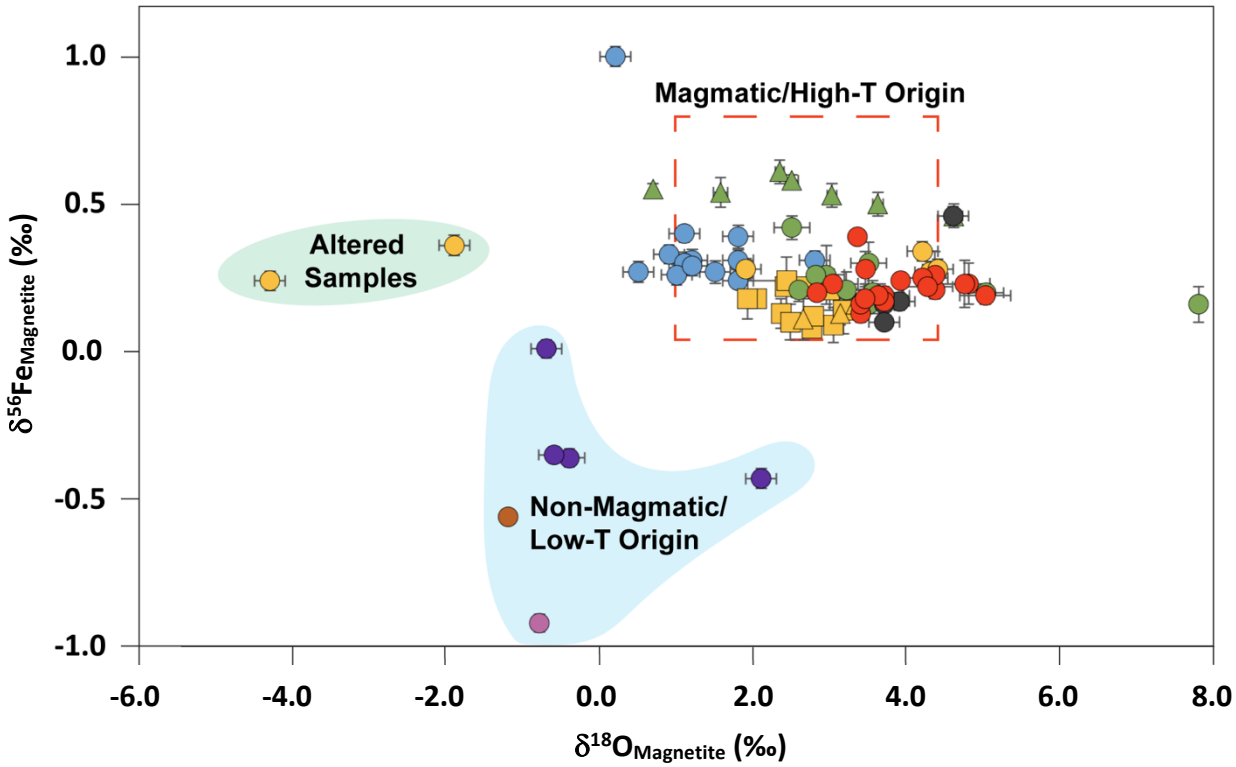

Figure 20. δ^{56}Fe and δ^{18}O pairs for magnetite from various deposit types. Shaded areas highlight samples altered samples and samples with a non-magmatic origin. The red box illustrates the magmatic range as defined by Taylor et al. (1967), Taylor (1968), Bindeman (2008), and Heimann et al. (2008). (1) Weis, 2013 (2) Troll et al., 2019 (3) Rodriguez-Mustafa et al., 2020 (4) Childress et al., 2020 (5) Bilenker et al., 2016; plot modified from Bilenker et al., 2016.

Deposit Type	Deposit, Location
Iron Skarn	Tibes, Puerto Rico
	Dannemora, Sweden[1,2]
IOCG	Candelaria, Chile[3]
	Mantoverde, Chile[4]
Chilean IOA	El Laco, Chile[1]
	Quince, Chile[3]
	Los Colorados, Chile[5]
Swedish IOA	Grangesberg Mining District, Sweden[4]
Other IOA	Mineville, New York[5]
Reference	Igneous Reference Material[1]
BIF	Striberg, Sweden[1]

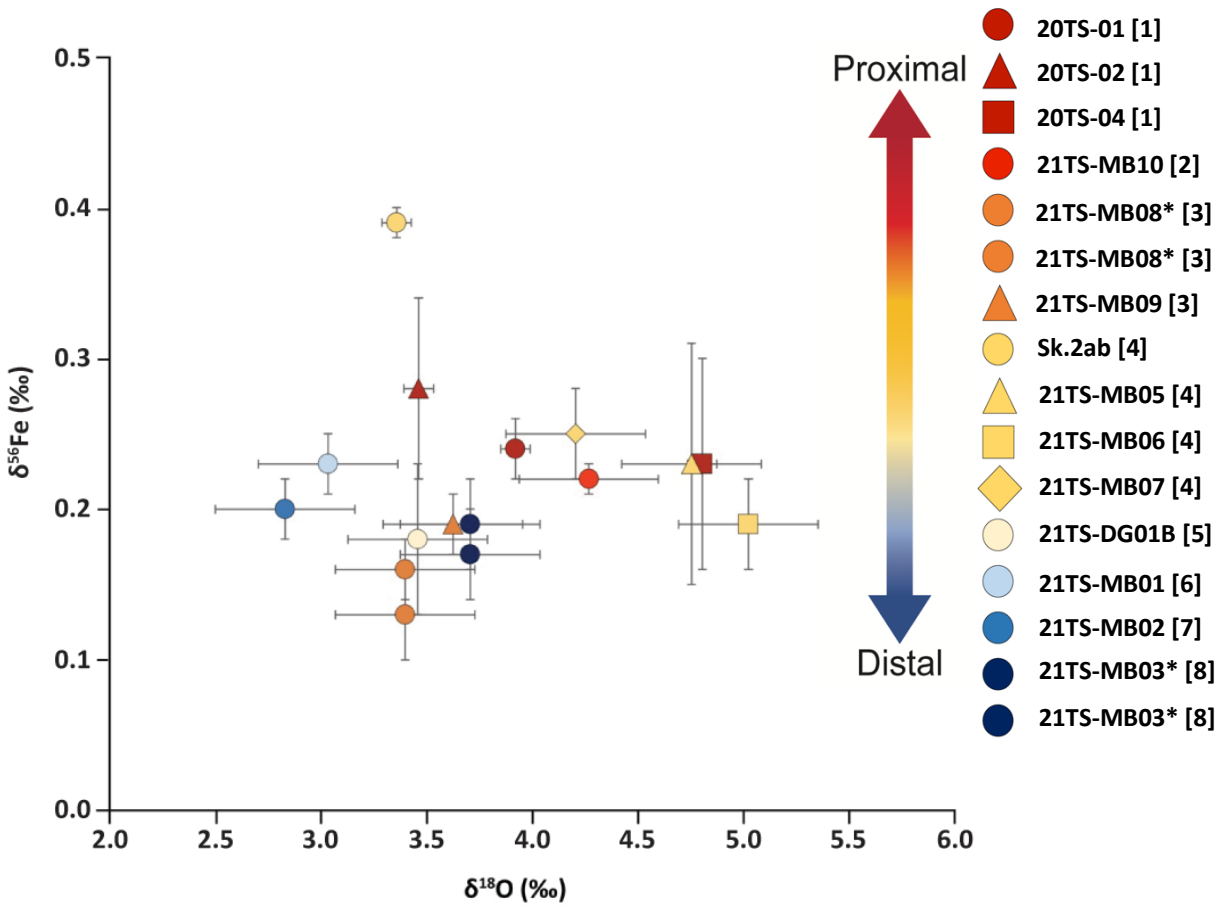

Figure 21. δ^{56}Fe and δ^{18}O isotope pairs for Tibes magnetite. The same color is used for samples from the same ore body, and different shapes are used for individual samples. The ore body number is indicated in brackets at the end of the sample name. 2σ errors are reported. Asterisks indicate samples duplicated for Fe isotope analyses; only one O isotope value exists.

11. The Formation of the Tibes Deposit

The formation of the Tibes iron skarn began with the intrusion of the Tibes Stock ~60 Ma (Pérez, 2008). Igneous activity in Puerto Rico was pervasive during the Late Cretaceous, and many of the island's intrusive bodies were emplaced during this time (Schellekens, 1998). As the pluton cooled, acidic magmatic-hydrothermal fluids rich in Fe and Si were released episodically. Magmatic Fe-O isotope signatures indicate that these fluids were the source of the magnetite ore. The carbonate host rock acted as a buffer for acidic fluids leaving the stock, causing an increase in pH and a decrease in the solubility of Si and Fe as the carbonate dissolved. This change in fluid conditions resulted in the precipitation of micron-scale silicate minerals, which were incorporated into precipitating magnetite grains (Figure 22; Robb, 2005; Meinert et al., 2005). The oscillatory nature of the zoning implies that episodic injections of additional acidic magmatic-hydrothermal fluids from the stock intermittently remobilized Si.

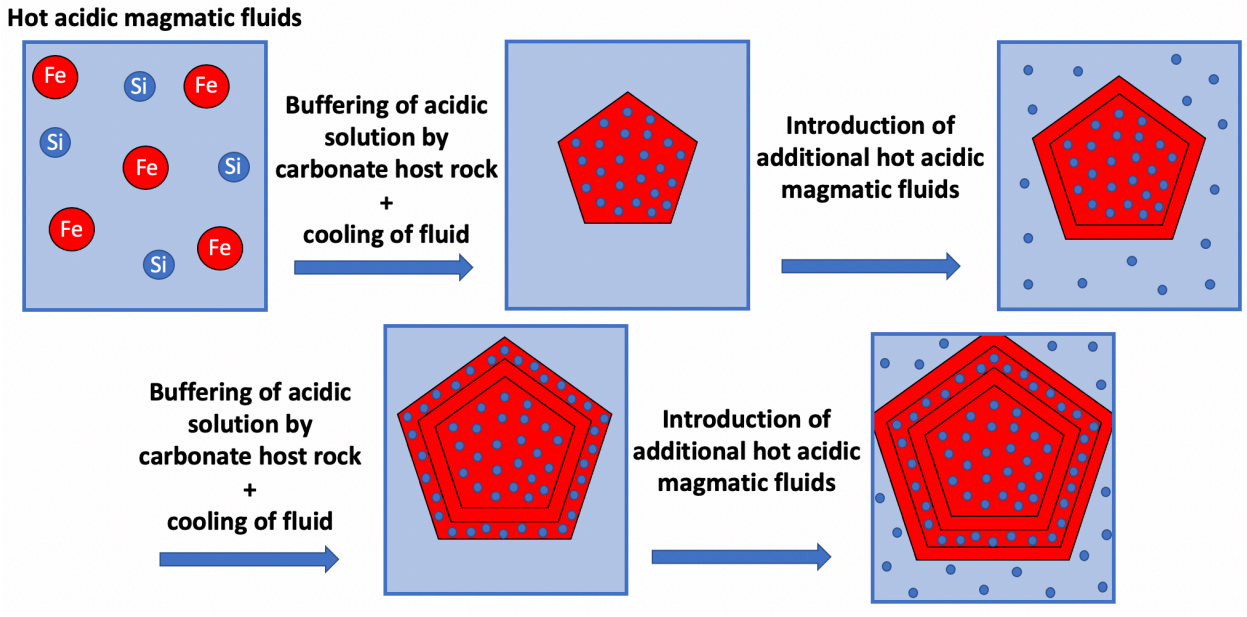

Figure 22. Simplified model for the formation of oscillatory zones of silicate micro-inclusions seen in Tibes magnetite.

The positive correlation between Ca and Si concentrations throughout the zoning in magnetite (Figure 17) supports neutralization by carbonate dissolution as a trigger for ore precipitation. Additionally, the magmatic O isotope signatures are evidence that the deposition of ore was not controlled by an influx of meteoric water, as is commonly the case for skarn deposits.

As fluids traveled away from the diorite stock (currently to the southeast of the Tibes skarn; Figure 9), fluid flow pathways were controlled by more permeable layers within the host rock, such as bedding planes or lithological boundaries. This is supported by the observation of linear N-NW trending magnetite ore bodies in sharp contact with the surrounding host rock (Figure 23). The physical concentration of fluid flow may have also been facilitated by localized faults, which were mapped by Krushensky and Monroe (1978) to have similar orientations as the ore bodies (Figure 9). However, no evidence for this was noted during field work for this study where observations were complicated by heavy vegetation. Future extensive mapping is required to confirm either of these possibilities.

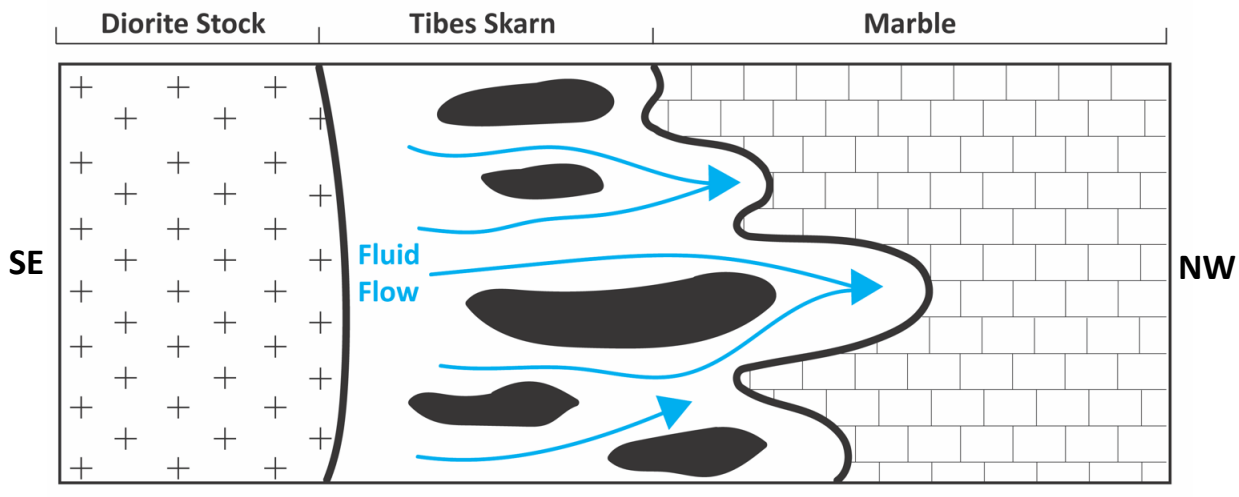

Figure 23. Simplified map view schematic of the directed fluid flow from the Tibes Stock into the carbonate host rock, which produced the linear magnetite bodies observed at the Tibes deposit (modified from Meinert et al., 2005).

12. Future Work

The focus of this study was to characterize the magnetite ore of the Tibes skarn and determine how this deposit formed. However, there are several aspects of ore deposit formation that cannot be addressed through observations and geochemical analysis of only the magnetite ore. A full understanding of the formation of ore deposits is necessary for resource evaluation and future exploration for similar deposits on Puerto Rico and in other similar tectonic settings. First, although petrographic observations and elemental maps indicate oscillatory zoning of Tibes magnetite, the number and timing of mineralization events that formed the Tibes skarn cannot be constrained. One way to do this is to analyze the geochemistry of the garnet associated with magnetite at Tibes. Collaborators at UPRM are performing geochronology and trace element analysis of zoned garnet grains, as this has the power to illuminate individual episodes of fluid flow and quantify the timing of mineralization. Detailed mapping and characterization of the entire deposit, including the diorite stock and host rock, are also required to constrain the fluid flow history of the deposit and the controls on fluid composition and pathways. Understanding fluid and metal transport in the Tibes skarn system is needed to complete its genetic model.

There are two other Puerto Rican iron skarn locations, Keystone and Island Queen, neither of which have yet to be characterized. These deposits are separated from Tibes by an island-scale fault zone (Figure 24), and by comparing field observations and the geochemistry of the three deposits, we can link iron skarn formation and the tectonic history of Puerto Rico.

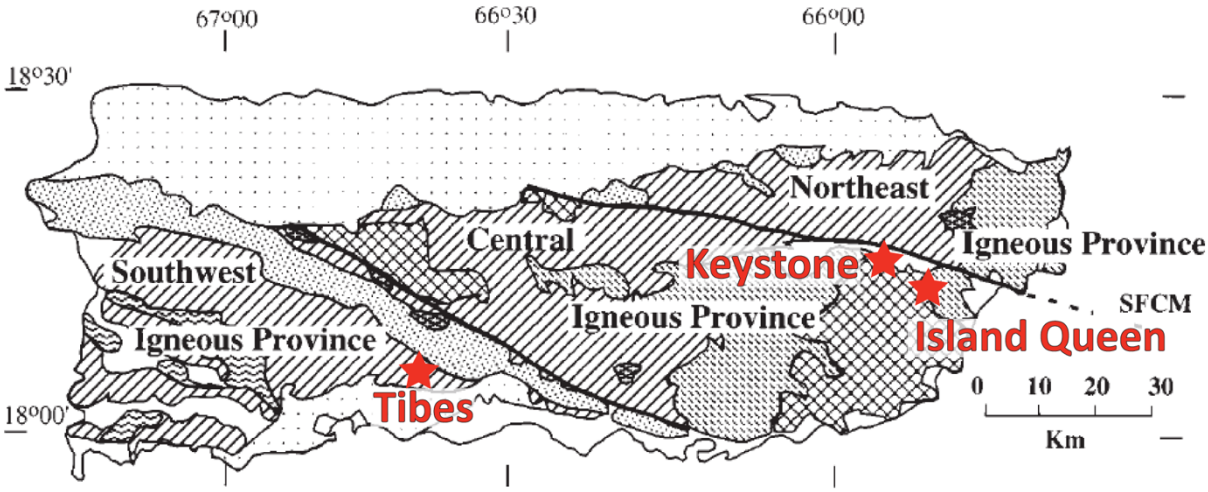

Figure 24. Approximate locations of the Tibes, Keystone, and Island Queen iron skarn deposits plotted on a geologic map of Puerto Rico (modified from Schellekens, 1998).

Preliminary field, isotopic, and trace element data indicate that magnetite ore present at each of the three deposits have had different sources and/or post depositional histories. Figure 25 displays the $\delta^{18}O$ values for magnetite from the three iron skarns and illustrates that magnetite from each deposit carries a distinct isotopic signature. Furthermore, Keystone and Island Queen are spatially associated with a Cu porphyry deposit while Tibes is not; this is an opportunity to investigate the factors that determine whether a porphyry deposit will form associated with a calcic iron skarn in an island arc setting.

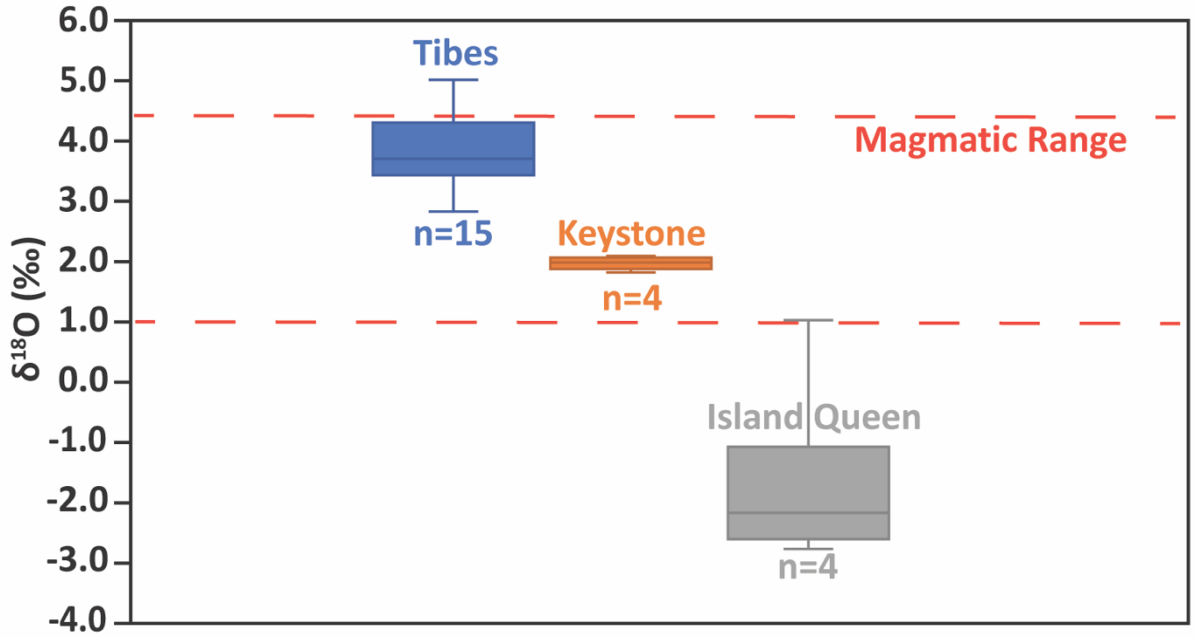

Figure 25. $\delta^{18}O$ values of magnetite from the Tibes iron deposit, Keystone Mine, and Island Queen Mine.

13. Conclusions

The combination of field observations with petrographic and geochemical analyses of magnetite ore has revealed the following about the Tibes iron skarn deposit in Puerto Rico:

- Deposition of linear magnetite bodies with sharp contacts are the result of directed magmatic-hydrothermal fluid flow controlled by differences in permeability (i.e., sedimentary bedding planes or lithological boundaries) or the presence of preexisting faults.
- Tibes magnetite has low concentrations of impurities including Ti and Cr, although some samples contained compositionally zoned grains.
- Trace element concentrations for Tibes magnetite are consistent with existing data for magnetite from other iron skarns. Variations in magnetite trace element concentrations

between ore bodies, within individual samples, and across the deposit highlight the importance of strategic deposit scale sample collection.

- Oscillatory zoning of silicate micro-inclusions within Tibes magnetite was produced by episodic fluctuations in fluid conditions during magnetite precipitation, due to progressive reactions between the fluid and host rock and/or multiple events of magmatic fluid release.
- Tibes magnetite has δ^{56}Fe and δ^{18}O isotopic signatures that are heavier than other skarn and hydrothermal deposits, reflecting a direct magmatic source and minimal meteoric water input or later alteration.
- Discrepancies between Tibes isotopic data and that of other iron skarns can be explained by:
    (1) Lack of accretion and metamorphism experienced by the Tibes iron skarn
    (2) Global data gap for isotope data for magnetite from iron skarns
- More detailed field observations and measurements along with geochemical analysis of other minerals (e.g., garnet), the diorite stock, and host rock need to be made across the entire Tibes skarn to understand the full geologic context for exploration and resource assessment purposes (e.g., link between island-scale faults and mineralization).

References

Bawiec, W. J., Alonzo, R., Cox, D., Griscom, A., Lipin, B., Marsh, S., McKelvey, G., Page, N., & Schellekens, J. H. (1999). Mineral Resource Assessment of Puerto Rico. In *Geology, geochemistry, geophysics, mineral occurrences and mineral resource assessment of the Commonwealth of Puerto Rico. U.S Geological Survey Open-File Report 98-38*.

Bawiec, W. J., Cox, D., McKelvey, G., Griscom, A., & Marsh, S. (1998). Mineral Deposit Summary Sheets. In *Geology, geochemistry, geophysics, mineral occurrences and mineral resource assessment of the Commonwealth of Puerto Rico. U.S Geological Survey Open-File Report 98-38*.

Bilenker, L. D., Simon, A. C., Reich, M., Lundstrom, C. C., Gajos, N., Bindeman, I., Barra, F., & Munizaga, R. (2016). Fe-O stable isotope pairs elucidate a high-temperature origin of Chilean iron oxide-apatite deposits. *Geochimica et Cosmochimica Acta*, *177*, 94–104. https://doi.org/10.1016/j.gca.2016.01.009

Bilenker, L. D., VanTongeren, J. A., Lundstrom, C. C., & Simon, A. C. (2017). Iron isotopic evolution during fractional crystallization of the uppermost Bushveld Complex layered mafic intrusion. *Geochemistry, Geophysics, Geosystems*, *18*(3), 956-972.

Bilenker, L. D., Weis, D., Scoates, J. S., & Perry, E. (2018). The application of stable Fe isotopes to magmatic sulfide systems: Constraints on the Fe isotope composition of magmatic pyrrhotite. *Economic Geology*, *113*(5), 1181–1192. https://doi.org/10.5382/econgeo.2018.4586

Bindeman, I. (2008). Oxygen isotopes in mantle and crustal magmas as revealed by single crystal analysis. *Reviews in Mineralogy and Geochemistry*, *69*, 445–478. https://doi.org/10.2138/rmg.2008.69.12

Byrne, D. B., Suarez, G., & McCann, W. R. (1985). Muertos Trough subduction—microplate tectonics in the northern Caribbean. *Nature*, *317*(6036), 420–421. https://doi.org/10.1038/317420a0

Childress, T. M., Simon, A. C., Reich, M., Barra, F., Arce, M., Lundstrom, C. C., & Bindeman, I. N. (2020). Formation of the Mantoverde iron oxide-copper-gold (IOCG) deposit, Chile: insights from Fe and O stable isotopes and comparisons with iron oxide-apatite (IOA) deposits. *Mineralium Deposita*, *55*(7), 1489–1504. https://doi.org/10.1007/s00126-019-00936-x

Cox, D., & Briggs, R. (1973). *Metallogenic Map of Puerto Rico* (Ser. 721). U.S. Geological Survey.

Craddock, P. R., & Dauphas, N. (2011). Iron isotopic compositions of geological reference materials and chondrites. *Geostandards and Geoanalytical Research*, *35*(1), 101-123.

Dare, S., Barnes, S. J., Beaudoin, G., Méric, J., Boutroy, E., & Potvin-Doucet, C. (2014). Trace elements in magnetite as petrogenetic indicators. *Mineralium Deposita*, *49.7*, 785–796.

Dolan, J., Mann, P., De Zoeten, R., Heubeck, C., Shiroma, J., & Monechi, S. (1991). Sedimentologie, stratigraphic, and tectonic synthesis of Eocene-Miocene sedimentary basins, Hispaniola and Puerto Rico. In *Special Paper of the Geological Society of America* (Vol. 262, pp. 217–263). https://doi.org/10.1130/SPE262-p217

Dupuis, C., & Beaudoin, G. (2011). Discriminant diagrams for iron oxide trace element fingerprinting of mineral deposit types. *Mineralium Deposita*, *46*(4), 319–335. https://doi.org/10.1007/s00126-011-0334-y

Duran, C. J., Barnes, S.-J., Mansur, E. T., Dare, S. A. S., Bédard, L. P., & Sluzhenikin, S. F. (2020). Magnetite Chemistry by Laser Ablation-Inductively Coupled Plasma-Mass Spectrometry Records Sulfide Fractional Crystallization in Massive Nickel-Copper-Platinum Group Element Ores from the Norilsk-Talnakh Mining District (Siberia, Russia): Implications for. *Economic Geology*, *Xx*. https://doi.org/10.5382/econgeo.4742

Elston, D., & Krushensky, R. (1983). Puerto Rico: A translated terrane exotic to the Caribbean (abs.). *10th Caribbean Geology Conference, Program and Abstracts of Papers*.

Gelabert, P. (2011). *Mineria en Puerto Rico*.

Giovannetti-Nazario, D., Hudgins, T. (2019). Field Relations and Magnetite Petrogenesis of the Tibes Skarn in Ponce, Puerto Rico [Unpublished Undergraduate Research]. University of Puerto Rico, Mayagüez.

Heimann, A., Beard, B. L., & Johnson, C. M. (2008). The role of volatile exsolution and sub-solidus fluid/rock interactions in producing high 56Fe/54Fe ratios in siliceous igneous rocks. *Geochimica et Cosmochimica Acta*, *72*(17), 4379-4396.

Huang, X. W., & Beaudoin, G. (2021). Nanoinclusions in zoned magnetite from the Sossego IOCG deposit, Carajás, Brazil: Implication for mineral zoning and magnetite origin discrimination. *Ore Geology Reviews*, 104453.

Johnson, C. M., Beard, B. L., Klein, C., Beukes, N. J., & Roden, E. E. (2008). Iron isotopes constrain biologic and abiologic processes in banded iron formation genesis. *Geochimica et Cosmochimica Acta*, *72*(1), 151-169.

Jolly, W. T., Lidiak, E. G., Schellekens, J. H., & Santos, H. (1998). Volcanism, tectonics, and stratigraphic correlations in Puerto Rico. In *Special Paper of the Geological Society of America* (Vol. 322, pp. 1–34). https://doi.org/10.1130/0-8137-2322-1.1

Kaye, C. (1957). Notes on the structural geology of Puerto Rico. *Bulletin of the Geological Society of America*, *68*, 103–118.

Knipping, J. L., Bilenker, L. D., Simon, A. C., Reich, M., Barra, F., Deditius, A. P., Wälle, M., Heinrich, C. A., Holtz, F., & Munizaga, R. (2015). Trace elements in magnetite from massive iron oxide-apatite deposits indicate a combined formation by igneous and magmatic-hydrothermal processes. *Geochimica et Cosmochimica Acta*, *171*, 15–38. https://doi.org/10.1016/j.gca.2015.08.010

Krushensky, R., & Monroe, W. (1978). Geologic map of the Peñuelas and Punta Chuchara

Quadrangles, Puerto Rico. U.S Geological Survey.

Krushensky, R., & Schellekens, J. H. (2001). Geology of Puerto Rico. In *Geology, geochemistry, geophysics, mineral occurrences and mineral resource assessment of the Commonwealth of Puerto Rico* (Open-File, pp. 25–40). U.S Geological Survey.

Larue, D. K. (1990). Toa Baja Drilling Project Puerto Rico. *Eos, Transactions American Geophysical Union*, *71*(5), 233–234. https://doi.org/10.1029/EO071i005p00233

Lindsley, D. (1991). Oxide Minerals: Petrologic and Magnetic Significance*. Reviews in Mineralogy*, 25.

Lutjen, G. P. (1971). The curious case of the Puerto Rican copper mines. *Engineering and Mining Journal*, *172*, 74–84.

Masson, D. G., & Scanlon, K. M. (1991). The neotectonic setting of Puerto Rico. *Geological Society of America Bulletin*, *103*(1), 144–154.

Meinert, L., Dipple, G., & Nicolescu, S. (2005). World Skarn Deposits. *Economic Geology*, *100th Anniversary Volume*, 299–336.

Minster, J. B., & Jordan, T. (1978). Present-day plate motions. *Journal of Geophysical Research*, *83(B11)*, 5331–5354.

Nadoll, P., Angerer, T., Mauk, J. L., French, D., & Walshe, J. (2014). The chemistry of hydrothermal magnetite: A review. *Ore Geology Reviews*, *61*, 1-32.

Nadoll, P., Mauk, J. L., Leveille, R. A., & Koenig, A. E. (2015). Geochemistry of magnetite from porphyry Cu and skarn deposits in the southwestern United States. *Mineralium Deposita*, *50*(4), 493–515. https://doi.org/10.1007/s00126-014-0539-y

Nelson, C. E., Proenza, J. A., Lewis, J. F., & López-Kramer, J. (2011). The metallogenic evolution of the Greater Antilles. *Geologica Acta*, *9*(3), 229–264. https://doi.org/10.1344/105.000001741

Pérez, R. J. (2008). *Oxygen isotope geochemistry of plutonic rocks from Puerto Rico [Master's Thesis]*. University of Puerto Rico, Mayagüez.

Pindell, J., Kennan, L., Stanek, K. P., Maresch, W. V., & Draper, G. (2006). Foundations of Gulf of Mexico and Caribbean evolution: Eight controversies resolved. *Geologica Acta*, *4*(1–2), 303–341. https://doi.org/10.1344/105.000000371

Pindell, J. L. (1994). Evolution of the Gulf of Mexico and the Caribbean. In *Caribbean geology: an introduction.* (pp. 13–39). U.W.I. Publishers' Association. https://doi.org/10.5724/gcs.01.21.0159

Pujols, E., & Cavosie, A. (2007). Geologic relations along the Rio Portugues near the Tibes stock contact aureole [Unpublished Undergraduate Research]. University of Puerto Rico, Mayagüez.

Rhodes, A. L., Oreskes, N., & Sheets, S. (1999). Geology and rare earth element geochemistry of magnetite deposits at El Laco, Chile. *Society of Economic Geologists Special Publication*, *7*, 299-332.

Robb, L. (2005). *Introduction to Ore-Forming Processes*. Blackwell Publishing.

Rodriguez-Mustafa, M. A., Simon, A. C., del Real, I., Thompson, J. F. H., Bilenker, L. D., Barra, F., Bindeman, I., & Cadwell, D. (2020). A Continuum from Iron Oxide Copper-Gold to Iron Oxide-Apatite Deposits: Evidence from Fe and O Stable Isotopes and Trace Element Chemistry of Magnetite. *Economic Geology*, *115*(7), 1443–1459. https://doi.org/10.5382/econgeo.4752

Schellekens, J. H. (1998). Geochemical evolution and tectonic history of Puerto Rico. In *Special Paper of the Geological Society of America* (Vol. 322). https://doi.org/10.1130/0-8137-2322-1.35

Simon, A. C., Knipping, J., Reich, M., Barra, F., Deditius, A. P., Bilenker, L., & Childress, T. (2019). Kiruna-Type Iron Oxide-Apatite (IOA) and Iron Oxide Copper-Gold (IOCG) Deposits Form by a Combination of Igneous and Magmatic-Hydrothermal Processes: Evidence from the Chilean Iron Belt. *Metals, Minerals, and Society*, *21*, 89–114. https://doi.org/10.5382/sp.21.06

Speed, R. C., & Larue, D. K. (1991). Extension and transtension in the plate boundary zone of the northeastern Caribbean. *Geophysical Research Letters*, *18*(3), 573–576.

Sykes, L. R., McCann, W. R., & Kafka, A. L. (1982). Motion of Caribbean plate during last 7 million years and implications for earlier Cenozoic movements. *Journal of Geophysical Research*, *87*(B13), 10656–10676. https://doi.org/10.1029/jb087ib13p10656

Taylor, H. P. (1968). The oxygen isotope geochemistry of igneous rocks. *Contributions to Mineralogy and Petrology*, *19*(1), 1–71. https://doi.org/10.1007/BF00371729

Taylor, H. P., Frechen, J., & Degens, E. T. (1967). Oxygen and carbon isotope studies of carbonatites from the Laacher See District, West Germany and the Alnö District, Sweden. *Geochimica et Cosmochimica Acta*, *31*(3), 407–430. https://doi.org/10.1016/0016-7037(67)90051-8

Troll, V. R., Weis, F. A., Jonsson, E., Andersson, U. B., Majidi, S. A., Högdahl, K., Harris, C., Millet, M. A., Chinnasamy, S. S., Kooijman, E., & Nilsson, K. P. (2019). Global Fe–O isotope correlation reveals magmatic origin of Kiruna-type apatite-iron-oxide ores. *Nature Communications*, *10*(1), 1–12. https://doi.org/10.1038/s41467-019-09244-4

U.S. Geological Survey. (2019). *Mineral Commodity Summaries 2019*. https://doi.org/10.3133/70202434

Vazquez, L. (1960). Geology and ore deposits of the Keystone iron mine near Juncos, Puerto Rico. *Department of Industrial Research, Economic Development Administration*, *Bulletin 7*.

Weis, F. (2013). Oxygen and Iron Isotope Systematics of the Grängesberg Mining District (GMD), Central Sweden (Issue 251). University of Uppsala.

Appendix A

Sample descriptions and GPS coordinates.

Sample	Ore Body	Type	Unit	Coordinates
Sk.2ab	4	Core	Magnetite Ore	18.080267°, -66.638350°
20TS-01	1	Core	Magnetite Ore	18.080426°, -66.638011°
20TS-02	1	Core	Magnetite Ore	18.080426°, -66.638011°
20TS-04.1	1	Hand Sample	Magnetite Ore	18.080426°, -66.638011°
20TS-04.2	1	Hand Sample	Magnetite Ore	18.080426°, -66.638011°
21TS-MB01	6	Core	Magnetite Ore	18.081317°, -66.638967°
21TS-MB02	7	Core	Magnetite Ore	18.081417°, -66.638983°
21TS-MB03	8	Core	Magnetite Ore	18.081683°, -66.639117°
21TS-MB04	-	Hand Sample	Dike	18.081417°, -66.638983°
21TS-MB05	4	Core	Magnetite Ore	18.080267°, -66.638350°
21TS-MB06	4	Core	Magnetite Ore	18.080267°, -66.638350°
21TS-MB07	4	Core	Magnetite Ore	18.080267°, -66.638350°
21TS-MB08	3	Core	Magnetite Ore	18.080373°, -66.638062°
21TS-MB09	3	Hand Sample	Magnetite Ore	18.080373°, -66.638062°
21TS-MB10	2	Core	Magnetite Ore	18.080383°, -66.638083°
21TS-MB11	-	Hand Sample	Tibes Diorite	18.080367°, -66.636200°
21TS-DG01B	5	Core	Magnetite Ore	18.081200°, -66.639100°

Appendix B

Major and trace and element data measured by electron microprobe. All concentrations reported in elemental wt%. Grey shading groups analyses of the same sample.

Sample	Mg	Al	Si	Ca	Ti	Cr	Fe*	Mn	Na	Nb	O	Total
Sk.2ab (1)	0.24	0.13	0.84	0.33	0.06	0.01	69.45	0.07	0.28	0.02	28.06	99.49
Sk.2ab (2)	0.14	0.20	1.19	0.54	0.03	0.00	67.42	0.15	0.00	0.03	27.68	97.38
Sk.2ab (2)	0.05	0.22	0.55	0.33	0.02	0.02	68.17	0.07	0.13	0.01	27.12	96.69
Sk.2ab (3)	0.06	0.29	0.07	0.14	0.02	0.00	69.38	0.07	0.00	0.03	27.00	97.08
Sk.2ab (4)	0.01	0.17	0.07	0.10	0.07	0.00	69.76	0.12	0.01	0.04	27.03	97.37
Sk.2ab (4)	0.07	0.17	0.35	0.09	0.04	0.00	69.97	0.10	0.46	0.01	27.58	98.84
Sk.2ab (5)	0.14	0.31	0.81	0.24	0.05	0.00	68.85	0.11	0.00	0.04	27.78	98.34
Sk.2ab (6)	0.00	0.07	0.00	0.02	0.03	0.03	70.56	0.14	0.00	0.03	27.11	97.99
Sk.2ab (7)	0.06	0.00	0.39	0.24	0.08	0.02	70.03	0.04	0.00	0.03	27.42	98.29
20TS-01	0.00	0.20	0.92	0.07	0.02	0.01	68.72	0.11	0.44	0.01	27.72	98.22
20TS-01	0.00	0.03	0.93	0.10	0.01	0.00	69.56	0.06	0.15	0.00	27.77	98.61
20TS-01	0.03	0.00	0.57	0.05	0.01	0.00	69.09	0.06	0.00	0.00	27.11	96.92
20TS-01	0.01	0.11	0.27	0.01	0.00	0.01	71.84	0.10	0.00	0.00	27.90	100.27
20TS-01	0.02	0.11	1.05	0.09	0.00	0.00	68.62	0.12	0.00	0.00	27.59	97.61
20TS-01	0.05	0.57	1.32	0.12	0.01	0.01	67.25	0.13	0.13	0.01	27.88	97.49
20TS-01	0.02	0.17	1.08	0.09	0.01	0.00	68.04	0.12	0.27	0.01	27.57	97.39
20TS-01	0.00	0.16	0.56	0.06	0.00	0.01	69.56	0.02	0.12	0.00	27.43	97.92
20TS-01	0.00	0.05	0.40	0.06	0.01	0.01	69.99	0.04	0.31	0.00	27.39	98.26
20TS-01	0.00	0.06	0.01	0.00	0.01	0.01	70.19	0.11	0.00	0.00	26.91	97.30
20TS-01	0.03	0.03	0.00	0.00	0.00	0.01	70.73	0.01	0.00	0.00	27.07	97.86
20TS-01	0.03	0.00	0.00	0.00	0.00	0.00	71.07	0.11	0.04	0.00	27.21	98.46
20TS-02 mgt	0.20	0.19	1.74	0.71	0.07	0.00	67.01	0.13	0.00	0.02	28.27	98.35
20TS-02 mgt(2)	0.21	0.24	2.02	0.81	0.09	0.00	66.64	0.12	0.20	0.03	28.62	98.98
20TS-02 mgt(3)	0.00	0.00	0.64	0.03	0.03	0.00	70.86	0.10	0.00	0.02	27.87	99.56
20TS-02 mgt(4)	0.14	0.13	1.11	0.49	0.03	0.00	69.08	0.09	0.00	0.02	28.11	99.20
20TS-02 mgt(6)	0.21	0.17	1.24	0.59	0.06	0.00	69.63	0.06	0.16	0.00	28.65	100.78
20TS-02 mgt(8)	0.03	0.20	0.33	0.15	0.05	0.01	71.23	0.16	0.54	0.02	28.14	100.86
20TS-02 mgt(9)	0.07	0.12	0.21	0.04	0.06	0.03	71.48	0.08	0.00	0.01	27.80	99.89
20TS-04.1(6)	0.31	0.13	2.24	0.88	0.06	0.01	67.40	0.09	0.00	0.01	29.05	100.18
20TS-04.1(7)	0.31	0.35	1.74	0.78	0.04	0.00	68.66	0.12	0.22	0.03	29.19	101.44

*Fe wt% represents total Fe. Analysis computer optimized to balance FeO and Fe_2O_3.

Sample	Mg	Al	Si	Ca	Ti	Cr	Fe*	Mn	Na	Nb	O	Total
20TS-04.1mgt	0.00	0.01	0.28	0.02	0.02	0.01	71.81	0.03	0.00	0.04	27.82	100.05
20TS-04.1mgt(1)	0.00	0.01	0.00	0.00	0.03	0.04	71.69	0.06	0.00	0.04	27.48	99.36
20TS-04.1mgt(2)	0.05	0.13	0.48	0.11	0.08	0.01	71.57	0.06	0.18	0.03	28.23	100.93
20TS-04.1mgt(3)	0.02	0.00	0.10	0.03	0.02	0.03	71.75	0.14	0.00	0.03	27.63	99.75
20TS-04.1mgt(4)	0.00	0.20	0.21	0.03	0.04	0.00	72.07	0.08	0.00	0.01	28.02	100.65
20TS-04.1 mgt(5)	0.00	0.14	0.53	0.04	0.00	0.00	71.27	0.06	0.00	0.01	27.99	100.02
20TS-04.1 mgt(8)	0.03	0.23	0.12	0.01	0.03	0.00	71.38	0.12	0.00	0.01	27.69	99.63
20TS-04.1 mgt(9)	0.00	0.14	1.38	0.14	0.02	0.00	68.51	0.11	0.51	0.01	28.16	98.99
20TS-04.2(1)	0.00	0.21	0.12	0.03	0.02	0.00	71.35	0.12	0.05	0.00	27.66	99.56
20TS-04.2(2)	0.00	0.14	0.46	0.02	0.02	0.01	70.26	0.06	0.01	0.00	27.53	98.52
20TS-04.2(6)	0.03	0.09	1.56	0.16	0.02	0.01	69.23	0.11	0.33	0.01	28.56	100.10
20TS-04.2(5)	0.00	0.19	1.52	0.15	0.01	0.00	67.58	0.11	0.00	0.00	27.81	97.36
20TS-04.2(5)	0.01	0.13	1.77	0.17	0.02	0.02	66.51	0.06	0.00	0.01	27.66	96.36
20TS-04.2(5)	0.02	0.06	1.49	0.14	0.01	0.00	67.05	0.06	0.07	0.00	27.48	96.38
20TS-04.2(4)	0.05	0.00	0.70	0.10	0.00	0.00	69.07	0.04	0.00	0.00	27.26	97.21
20TS-04.2(9)	0.00	0.18	0.00	0.00	0.01	0.00	70.28	0.12	0.00	0.00	27.05	97.64
20TS-04.2(10)	0.03	0.42	1.27	0.09	0.02	0.00	68.92	0.07	0.00	0.00	28.24	99.05
21TS-MB01 (2)	0.17	0.20	0.87	0.25	0.03	0.00	68.64	0.11	0.00	0.05	27.67	97.97
21TS-MB01 (2)	0.02	0.13	0.18	0.15	0.04	0.00	69.63	0.07	0.06	0.02	27.08	97.38
21TS-MB01(2)	0.13	0.18	0.61	0.20	0.00	0.00	69.14	0.03	0.32	0.02	27.56	98.18
21TS-MB01(1)	0.00	0.04	0.60	0.21	0.01	0.00	70.62	0.04	0.00	0.03	27.82	99.37
21TS-MB01(3)	0.00	0.24	0.84	0.07	0.03	0.03	68.88	0.01	0.00	0.03	27.56	97.68
21TS-MB01(3)	0.12	0.22	0.74	0.21	0.00	0.01	68.36	0.06	0.00	0.03	27.36	97.12
21TS-MB01(3)	0.00	0.17	0.73	0.08	0.03	0.00	68.42	0.08	0.45	0.03	27.37	97.35
21TS-MB01(3)	0.08	0.18	0.84	0.08	0.02	0.02	68.92	0.04	0.00	0.02	27.57	97.77
21TS-MB01(4)	0.11	0.19	1.09	0.35	0.03	0.04	67.50	0.05	0.00	0.02	27.47	96.84
21TS-MB01(4)	0.08	0.56	1.44	0.18	0.00	0.00	66.18	0.06	0.00	0.02	27.58	96.10
21TS-MB01(4)	0.06	0.13	0.52	0.22	0.01	0.01	67.82	0.07	0.55	0.02	26.97	96.37
21TS-MB01(4)	0.14	0.08	0.77	0.25	0.02	0.02	67.57	0.10	0.19	0.00	27.08	96.24

*Fe wt% represents total Fe. Analysis computer optimized to balance FeO and Fe_2O_3.

Sample	Mg	Al	Si	Ca	Ti	Cr	Fe*	Mn	Na	Nb	O	Total
21TS-MB01(5)	0.05	0.20	0.33	0.21	0.01	0.00	69.53	0.04	0.15	0.00	27.30	97.82
21TS-MB01(5)	0.12	0.19	0.46	0.24	0.02	0.00	68.98	0.10	0.00	0.01	27.26	97.38
21TS-MB02(1)	0.20	0.30	1.22	0.23	0.03	0.00	68.46	0.08	0.00	0.02	28.09	98.63
21TS-MB02(2)	0.34	0.42	1.47	0.42	0.04	0.00	69.14	0.16	0.00	0.00	28.92	100.90
21TS-MB02(3)	0.00	0.17	0.28	0.02	0.04	0.00	71.16	0.05	0.14	0.02	27.76	99.64
21TS-MB02(4)	0.04	0.15	0.18	0.01	0.01	0.03	70.88	0.12	0.00	0.03	27.53	99.00
21TS-MB02(5)	0.13	0.31	0.63	0.18	0.03	0.01	68.90	0.10	0.18	0.04	27.60	98.09
21TS-MB03(1)	0.12	0.22	0.75	0.23	0.00	0.02	68.31	0.11	0.04	0.02	27.38	97.18
21TS-MB03(2)	0.04	0.23	0.14	0.08	0.02	0.02	67.25	0.08	0.00	0.02	26.17	94.04
21TS-MB03(3)	0.04	0.09	0.38	0.12	0.03	0.04	67.58	0.03	0.00	0.01	26.45	94.77
21TS-MB03(4)	0.09	0.20	0.00	0.04	0.01	0.00	70.24	0.08	0.00	0.01	27.12	97.79
21TS-MB03(7)	0.04	0.27	0.23	0.06	0.01	0.00	68.08	0.10	0.00	0.02	26.61	95.43
21TS-MB03(7)	0.05	0.07	0.08	0.04	0.02	0.00	69.25	0.12	0.21	0.01	26.79	96.65
21TS-MB05(1)	0.09	0.26	0.20	0.10	0.05	0.02	70.72	0.04	0.00	0.02	27.63	99.13
21TS-MB05(2)	0.00	0.01	0.03	0.16	0.05	0.00	71.51	0.10	0.00	0.02	27.51	99.41
21TS-MB05(3)	0.08	0.16	0.03	0.08	0.06	0.03	70.06	0.08	0.00	0.03	27.11	97.70
21TS-MB05(4)	0.33	0.42	1.63	0.68	0.06	0.03	67.92	0.20	0.00	0.03	28.79	100.08
21TS-MB05(5)	0.02	0.03	0.03	0.05	0.04	0.00	71.16	0.05	0.00	0.03	27.33	98.74
21TS-MB05(6)	0.07	0.00	0.42	0.31	0.07	0.01	70.92	0.10	0.00	0.02	27.83	99.75
21TS-MB06(1)	0.26	0.40	1.04	0.18	0.05	0.03	67.78	0.16	0.43	0.03	27.93	98.27
21TS-MB06(2)	0.06	0.21	0.31	0.08	0.00	0.00	69.52	0.07	0.00	0.02	27.20	97.46
21TS-MB06(3)	0.05	0.18	0.26	0.09	0.03	0.01	69.15	0.10	0.10	0.01	27.03	97.01
21TS-MB06(4)	0.22	0.46	1.11	0.41	0.02	0.00	66.66	0.15	0.00	0.01	27.50	96.54
21TS-MB06(5)	0.08	0.24	0.30	0.13	0.02	0.00	67.22	0.04	0.17	0.02	26.43	94.66
21TS-MB06(6)	0.08	0.10	0.20	0.14	0.04	0.00	67.69	0.17	0.21	0.04	26.45	95.12
21TS-MB06(7)	0.17	0.80	1.45	0.50	0.06	0.02	65.01	0.11	0.48	0.02	27.76	96.38
21TS-MB07(1)	0.12	0.67	0.43	0.22	0.17	0.01	67.64	0.05	0.18	0.03	27.29	96.79
21TS-MB07(2)	0.06	0.22	0.18	0.13	0.10	0.01	67.26	0.07	0.00	0.04	26.31	94.39
21TS-MB07(3)	0.10	0.72	0.39	0.23	0.11	0.02	67.72	0.15	0.00	0.03	27.25	96.71

*Fe wt% represents total Fe. Analysis computer optimized to balance FeO and Fe_2O_3.

Sample	Mg	Al	Si	Ca	Ti	Cr	Fe*	Mn	Na	Nb	O	Total
21TS-MB07(5)	0.10	0.80	0.31	0.21	0.10	0.04	66.01	0.02	0.24	0.03	26.62	94.49
21TS-MB07(5)	0.05	0.03	0.00	0.06	0.08	0.02	69.23	0.08	0.40	0.04	26.78	96.78
21TS-MB07(4)	0.03	0.33	0.00	0.15	0.10	0.00	67.57	0.12	0.29	0.04	26.41	95.03
21TS-MB07(6)	0.00	0.16	0.00	0.08	0.08	0.02	69.90	0.04	0.00	0.03	26.97	97.27
21TS-MB08(1)	0.10	0.05	0.45	0.12	0.03	0.02	68.13	0.10	0.07	0.04	26.80	95.90
21TS-MB08(1)	0.06	0.06	0.28	0.10	0.07	0.00	68.21	0.09	0.00	0.02	26.59	95.46
21TS-MB08(1)	0.34	0.54	2.02	0.63	0.06	0.02	64.98	0.17	0.00	0.03	28.20	96.99
21TS-MB08(2)	0.16	0.21	0.84	0.46	0.06	0.01	67.28	0.09	0.23	0.01	27.29	96.63
21TS-MB08(3)	0.00	0.30	0.04	0.01	0.02	0.03	69.16	0.10	0.35	0.03	26.93	96.97
21TS-MB08(4)	0.27	0.28	1.46	0.61	0.07	0.02	66.07	0.17	0.40	0.03	27.83	97.21
21TS-MB08(5)	0.02	0.11	0.00	0.02	0.04	0.03	68.73	0.18	0.01	0.03	26.49	95.68
21TS-MB08(6)	0.28	0.54	1.73	0.71	0.02	0.02	66.16	0.16	0.00	0.01	28.26	97.87
21TS-MB08(7)	0.33	0.40	1.20	0.38	0.07	0.00	67.63	0.15	0.30	0.02	28.14	98.63
21TS-MB09(1)	0.45	0.77	1.72	0.71	0.03	0.02	67.34	0.18	0.36	0.01	29.16	100.74
21TS-MB09(2)	0.01	0.05	0.04	0.11	0.06	0.01	71.80	0.06	0.06	0.02	27.66	99.88
21TS-MB09(3)	0.01	0.14	0.14	0.15	0.03	0.02	71.51	0.04	0.29	0.00	27.81	100.14
21TS-MB09(4)	0.05	0.17	0.69	0.21	0.04	0.02	71.50	0.07	0.30	0.02	28.54	101.62
21TS-MB09(5)	0.16	0.25	0.85	0.28	0.02	0.00	69.67	0.10	0.00	0.01	28.07	99.41
21TS-MB09(6)	0.03	0.07	0.16	0.13	0.00	0.00	70.90	0.06	0.04	0.02	27.44	98.85
21TS-MB10(1)	0.00	0.02	0.06	0.07	0.04	0.03	70.76	0.07	0.18	0.02	27.29	98.55
21TS-MB10(2)	0.13	0.05	0.43	0.08	0.05	0.02	70.33	0.00	0.59	0.04	27.79	99.52
21TS-MB10(5)	0.09	0.21	0.89	0.28	0.06	0.02	68.42	0.12	0.18	0.02	27.66	97.94
21TS-MB10(1.1)	0.01	0.09	0.15	0.03	0.04	0.06	71.33	0.04	0.00	0.02	27.59	99.36
21TS-MB10(4.1)	0.00	0.18	0.54	0.19	0.06	0.00	69.51	0.08	0.00	0.03	27.47	98.05
DG01B(1)	0.02	0.10	0.00	0.02	0.00	0.00	70.48	0.05	0.00	0.03	27.06	97.76
DG01B(2)	0.04	0.21	0.00	0.21	0.03	0.00	69.48	0.07	0.27	0.02	26.98	97.30
DG01B(3)	0.01	0.21	0.00	0.05	0.03	0.00	69.71	0.00	0.01	0.02	26.89	96.94
DG01B(3)	0.01	0.00	0.00	0.02	0.02	0.00	70.11	0.03	0.12	0.00	26.86	97.16
DG01B(4)	0.01	0.12	0.37	0.03	0.00	0.00	69.97	0.01	0.16	0.02	27.35	98.04
DG01B(5)	0.07	0.18	0.32	0.13	0.02	0.00	69.04	0.05	0.14	0.01	27.07	97.02
DG01B(6)	0.01	0.12	0.06	0.01	0.01	0.00	70.60	0.06	0.14	0.02	27.24	98.28

*Fe wt% represents total Fe. Analysis computer optimized to balance FeO and Fe_2O_3.

Sample	Mg	Al	Si	Ca	Ti	Cr	Fe	Mn	Na	Nb	O	Total
USNM 114887	0.06	0.02	0.01	0.01	0.04	0.02	72.19	0.06	0.00	0.19	27.81	100.40
USNM 114887	0.04	0.00	0.00	0.00	0.02	0.01	71.95	0.07	0.00	0.20	27.69	100.00
USNM 114887	0.02	0.00	0.00	0.00	0.04	0.01	71.72	0.10	0.39	0.17	27.71	100.16
USNM 114887	0.00	0.00	0.00	0.00	0.00	0.00	71.60	0.07	0.09	0.03	27.42	99.21
USNM 114887	0.00	0.00	0.00	0.02	0.02	0.01	71.64	0.06	0.33	0.04	27.55	99.66
USNM 114887	0.00	0.09	0.16	0.00	0.02	0.00	71.30	0.08	0.04	0.03	27.56	99.27
USNM 114887	0.04	0.00	0.00	0.00	0.02	0.00	71.35	0.10	0.00	0.04	27.35	98.91
USNM 114887	0.00	0.00	0.00	0.00	0.01	0.00	71.42	0.12	0.00	0.03	27.35	98.94
USNM 114887	0.00	0.00	0.00	0.00	0.01	0.01	72.37	0.07	0.00	0.04	27.69	100.18
USNM 114887	0.06	0.00	0.02	0.01	0.01	0.00	71.63	0.08	0.00	0.03	27.48	99.32
USNM 114887	0.00	0.00	0.04	0.00	0.03	0.00	71.89	0.10	0.20	0.03	27.65	99.96
USNM 114887	0.00	0.00	0.01	0.00	0.03	0.00	72.26	0.08	0.00	0.03	27.68	100.09
USNM 114887	0.00	0.00	0.06	0.00	0.02	0.00	71.84	0.03	0.00	0.03	27.55	99.54
USNM 114887	0.02	0.08	0.00	0.00	0.02	0.01	71.43	0.05	0.00	0.03	27.42	99.05
USNM 114887	0.06	0.00	0.00	0.00	0.00	0.00	71.02	0.05	0.06	0.04	27.23	98.46
USNM 114887	0.00	0.10	0.00	0.00	0.01	0.00	72.31	0.12	0.20	0.03	27.84	100.61
USNM 114887	0.00	0.00	0.11	0.00	0.01	0.00	72.32	0.03	0.35	0.03	27.91	100.76
USNM 114887	0.00	0.01	0.02	0.00	0.01	0.00	72.47	0.08	0.19	0.03	27.82	100.62
USNM 114887	0.03	0.00	0.00	0.00	0.02	0.00	72.12	0.08	0.00	0.03	27.62	99.89
USNM 114887	0.00	0.00	0.01	0.01	0.01	0.01	72.62	0.07	0.00	0.04	27.81	100.58
USNM 114887	0.00	0.08	0.00	0.01	0.03	0.00	71.94	0.05	0.00	0.04	27.61	99.76
USNM 114887	0.00	0.02	0.00	0.00	0.00	0.00	72.84	0.05	0.00	0.04	27.89	100.86
USNM 114887	0.05	0.00	0.00	0.03	0.08	0.01	71.01	0.07	0.36	0.19	27.49	99.29
USNM 114887	0.07	0.00	0.00	0.01	0.06	0.00	71.71	0.06	0.08	0.20	27.65	99.84
USNM 114887	0.02	0.00	0.03	0.03	0.07	0.00	72.05	0.05	0.42	0.18	27.90	100.74
USNM 114887	0.00	0.05	0.00	0.03	0.09	0.00	72.26	0.06	0.00	0.20	27.86	100.55
USNM 114887	0.03	0.01	0.00	0.00	0.08	0.02	72.53	0.06	0.00	0.22	27.96	100.91
USNM 114887	0.03	0.00	0.00	0.00	0.21	0.01	72.30	0.15	0.00	0.20	27.95	100.86
USNM 114887	0.08	0.00	0.00	0.02	0.09	0.00	71.35	0.05	0.18	0.18	27.57	99.52
USNM 114887	0.02	0.05	0.00	0.03	0.14	0.00	70.92	0.11	0.00	0.19	27.41	98.86

*Fe wt% represents total Fe. Analysis computer optimized to balance FeO and Fe_2O_3.

Sample	Mg	Al	Si	Ca	Ti	Cr	Fe	Mn	Na	Nb	O	Total
USNM 114887	0.10	0.04	0.00	0.01	0.13	0.01	71.37	0.04	0.11	0.21	27.63	99.64
USNM 114887	0.07	0.00	0.07	0.02	0.09	0.00	71.82	0.07	0.00	0.19	27.76	100.07
USNM 114887	0.06	0.06	0.00	0.00	0.79	0.00	70.56	0.33	0.00	0.25	27.83	99.89
USNM 114887	0.01	0.00	0.00	0.01	0.08	0.00	71.61	0.04	0.00	0.21	27.56	99.53
USNM 114887	0.05	0.00	0.00	0.00	0.09	0.03	71.47	0.07	0.03	0.22	27.57	99.51
USNM 114887	0.07	0.03	0.02	0.00	0.09	0.00	71.76	0.11	0.02	0.21	27.75	100.07
USNM 114887	0.12	0.00	0.00	0.02	0.19	0.00	72.29	0.15	0.00	0.22	28.01	101.00
USNM 114887	0.01	0.00	0.01	0.02	0.05	0.01	71.23	0.08	0.00	0.21	27.44	99.07
USNM 114887	0.05	0.08	0.00	0.05	0.09	0.00	70.83	0.04	0.00	0.23	27.39	98.74
USNM 114887	0.04	0.02	0.00	0.01	0.04	0.00	70.90	0.04	0.00	0.20	27.30	98.56
USNM 114887	0.01	0.06	0.01	0.01	0.07	0.01	71.22	0.03	0.25	0.20	27.55	99.41
USNM 114887	0.06	0.02	0.00	0.01	0.10	0.00	70.72	0.03	0.24	0.20	27.36	98.75
USNM 114887	0.13	0.00	0.04	0.00	0.31	0.01	70.68	0.13	0.07	0.21	27.54	99.13
USNM 114887	0.04	0.02	0.00	0.02	0.08	0.01	71.37	0.08	0.17	0.21	27.59	99.60
USNM 114887	0.07	0.00	0.05	0.02	0.07	0.02	72.05	0.08	0.32	0.23	27.97	100.87
20TS-01 light	0.0	0.2	1.2	0.5	0.0	0.0	69.0	0.1	0.1	0.0	28.2	99.4
20TS-01 dark	0.2	0.1	1.8	0.7	0.0	0.0	67.0	0.1	0.2	0.0	28.3	98.5
20TS-01 light	0.1	0.1	0.9	0.3	0.0	0.0	71.5	0.1	0.1	0.0	28.6	101.7
20TS-01 dark	0.2	0.2	1.9	0.8	0.0	0.0	67.7	0.1	0.0	0.0	28.8	99.8
20TS-01 light	0.0	0.0	0.0	0.1	0.0	0.0	71.1	0.1	0.0	0.0	27.3	98.8
20TS-01 dark	0.2	0.3	1.5	0.5	0.0	0.0	69.5	0.1	0.3	0.0	28.9	101.3
20TS-01 dark	0.2	0.1	1.5	0.7	0.0	0.0	68.6	0.1	0.0	0.0	28.5	99.7
20TS-01 light	0.3	0.4	1.3	0.5	0.0	0.0	67.6	0.1	0.2	0.0	28.1	98.4
20TS-01 dark	0.3	0.4	2.0	0.8	0.1	0.0	69.1	0.1	0.6	0.0	29.8	103.2
20TS-01 light	0.0	0.0	0.2	0.0	0.0	0.0	72.8	0.1	0.0	0.0	28.0	101.1
20TS-01 light	0.0	0.1	0.0	0.0	0.0	0.0	71.9	0.0	0.1	0.0	27.7	100.0

*Fe wt% represents total Fe. Analysis computer optimized to balance FeO and Fe_2O_3.

Appendix C

Trace element data measured by laser ablation inductively coupled plasma mass spectrometry. All concentrations are reported in wt%. Grey shading groups analyses of the same sample.

Sample	^{24}Mg	2SD	^{25}Mg	2SD	^{27}Al	2SD	^{29}Si	2SD	^{43}Ca	2SD	^{44}Ca	2SD	^{47}Ti	2SD	^{49}Ti	2SD	^{51}V	2SD
20TS-02 mgt	0.17	0.03	0.17	0.02	0.16	0.04	2.00	0.43	0.69	0.23	0.65	0.10	0.03	0.01	0.03	0.01	0.00	0.00
20TS-02 mgt(2)	0.12	0.03	0.12	0.03	0.19	0.04	1.62	0.48	0.47	0.22	0.45	0.12	0.03	0.00	0.03	0.01	0.00	0.00
20TS-02 mgt(3)	0.22	0.04	0.22	0.03	0.31	0.05	2.72	0.76	0.94	0.36	0.91	0.18	0.05	0.01	0.05	0.01	0.00	0.00
20TS-02 mgt(4)	0.14	0.05	0.14	0.06	0.12	0.05	1.73	0.79	0.58	0.40	0.55	0.27	0.03	0.01	0.03	0.01	0.00	0.00
20TS-02 mgt(6)	0.16	0.03	0.16	0.03	0.17	0.04	1.94	0.60	0.68	0.30	0.62	0.16	0.03	0.01	0.03	0.01	0.00	0.00
20TS-02 mgt(8)	0.11	0.04	0.10	0.03	0.35	0.12	1.44	0.40	0.22	0.13	0.21	0.09	0.03	0.01	0.03	0.01	0.00	0.00
20TS-02 mgt(9)	0.03	0.01	0.03	0.01	0.19	0.05	1.09	0.43	0.06	0.08	0.07	0.05	0.03	0.01	0.03	0.01	0.00	0.00
20TS-04.1 mgt(3)	0.07	0.03	0.06	0.02	0.16	0.05	0.94	0.59	0.21	0.21	0.21	0.10	0.05	0.01	0.05	0.01	0.00	0.00
20TS-04.1 mgt(4)	0.05	0.02	0.05	0.02	0.16	0.04	0.90	0.61	0.16	0.15	0.15	0.08	0.05	0.01	0.05	0.01	0.00	0.00
20TS-04.1 mgt(5)	0.21	0.11	0.19	0.04	0.20	0.20	1.84	0.93	0.82	0.29	0.70	0.20	0.03	0.02	0.04	0.03	0.00	0.00
20TS-04.1 mgt(6)	0.15	0.03	0.18	0.03	0.23	0.06	1.68	0.54	0.70	0.26	0.73	0.29	0.05	0.01	0.05	0.01	0.00	0.00
20TS-04.1 mgt(7)	0.11	0.05	0.10	0.03	0.26	0.10	1.51	0.89	0.32	0.19	0.29	0.10	0.04	0.01	0.05	0.02	0.00	0.00
20TS-04.1 mgt(8)	0.12	0.03	0.12	0.02	0.23	0.06	1.58	0.46	0.41	0.22	0.42	0.13	0.05	0.02	0.05	0.01	0.01	0.00
20TS-04.2 mgt(1)	0.04	0.01	0.04	0.01	0.19	0.02	0.84	0.31	0.10	0.11	0.10	0.04	0.03	0.01	0.03	0.00	0.00	0.00
20TS-04.2 mgt(2)	0.05	0.02	0.05	0.02	0.19	0.03	0.94	0.34	0.14	0.15	0.14	0.08	0.03	0.01	0.03	0.01	0.00	0.00
20TS-04.2 mgt(5)	0.18	0.07	0.20	0.07	0.23	0.11	1.80	0.69	0.73	0.35	0.76	0.34	0.03	0.01	0.03	0.01	0.00	0.00
20TS-04.2 mgt(6)	0.17	0.03	0.18	0.03	0.20	0.04	1.62	0.37	0.82	0.26	0.87	0.36	0.03	0.01	0.03	0.01	0.00	0.00
20TS-04.2 mgt(9)	0.05	0.03	0.05	0.03	0.24	0.06	0.93	0.31	0.11	0.14	0.11	0.11	0.03	0.01	0.03	0.01	0.00	0.00
20TS-04.2 mgt(10)	0.02	0.01	0.02	0.01	0.14	0.01	0.63	0.25	0.05	0.07	0.04	0.04	0.03	0.01	0.03	0.01	0.01	0.00
21TS-MB01 mgt	0.13	0.02	0.13	0.01	0.22	0.02	1.02	0.20	0.21	0.12	0.20	0.05	0.02	0.00	0.02	0.00	0.00	0.00
21TS-MB01 mgt(1)	0.10	0.01	0.10	0.01	0.20	0.02	0.72	0.17	0.17	0.12	0.17	0.04	0.01	0.00	0.01	0.00	0.00	0.00
21TS-MB01 mgt(2)	0.11	0.04	0.12	0.04	0.23	0.08	0.83	0.22	0.24	0.15	0.24	0.10	0.02	0.01	0.02	0.01	0.00	0.00
21TS-MB01 mgt(3)	0.09	0.01	0.09	0.01	0.23	0.02	0.87	0.18	0.30	0.15	0.29	0.04	0.02	0.00	0.02	0.00	0.00	0.00
21TS-MB01 mgt(4)	0.10	0.02	0.10	0.02	0.25	0.06	0.92	0.20	0.22	0.15	0.22	0.07	0.02	0.01	0.02	0.01	0.00	0.00
21TS-MB02 mgt(1)	0.29	0.04	0.29	0.03	0.29	0.05	1.06	0.24	0.36	0.16	0.36	0.06	0.02	0.00	0.02	0.00	0.00	0.00
21TS-MB02 mgt(2)	0.29	0.03	0.30	0.03	0.36	0.04	1.16	0.21	0.36	0.17	0.38	0.09	0.02	0.00	0.02	0.00	0.00	0.00
21TS-MB02 mgt(3)	0.39	0.07	0.33	0.05	0.53	0.13	1.37	0.27	0.40	0.15	0.36	0.09	0.03	0.01	0.03	0.01	0.00	0.00
21TS-MB02 mgt(4)	0.22	0.08	0.21	0.05	0.26	0.14	1.18	0.46	0.34	0.12	0.25	0.06	0.01	0.00	0.02	0.01	0.00	0.00
21TS-MB03 mgt1	0.11	0.05	0.11	0.05	0.18	0.03	0.54	0.16	0.19	0.12	0.18	0.06	0.00	0.00	0.01	0.00	0.00	0.00
21TS-MB03 mgt3	0.06	0.02	0.06	0.02	0.22	0.04	0.37	0.12	0.10	0.07	0.10	0.06	0.02	0.00	0.01	0.00	0.00	0.00
21TS-MB03 mgt4	0.05	0.01	0.05	0.01	0.20	0.07	0.33	0.17	0.07	0.10	0.04	0.06	0.00	0.00	0.00	0.00	0.00	0.00
21TS-MB03 mgt5	0.06	0.01	0.06	0.01	0.16	0.04	0.34	0.12	0.08	0.09	0.08	0.05	0.01	0.00	0.01	0.00	0.00	0.00
21TS-MB03 mgt6	0.05	0.03	0.05	0.03	0.20	0.06	0.43	0.17	0.11	0.12	0.10	0.06	0.02	0.01	0.02	0.01	0.00	0.00
21TS-MB03 mgt7	0.11	0.06	0.11	0.06	0.15	0.03	0.45	0.14	0.07	0.08	0.07	0.04	0.00	0.00	0.00	0.00	0.00	0.00

Sample	^{52}Cr	2SD	^{53}Cr	2SD	^{55}Mn	2SD	^{56}Fe	2SD	^{59}Co	2SD	^{60}Ni	2SD	^{71}Ga	2SD	Ti+V	Al+Mn+Ca
20TS-02 mgt	0.00	0.00	0.00	0.00	0.08	0.02	70.38	6.04	0.00	0.00	0.00	0.00	0.00	0.00	0.03	0.93
20TS-02 mgt(2)	0.00	0.00	0.00	0.00	0.11	0.01	71.09	6.61	0.00	0.00	0.00	0.00	0.00	0.00	0.03	0.77
20TS-02 mgt(3)	0.00	0.00	0.00	0.00	0.14	0.01	75.15	7.03	0.00	0.00	0.00	0.00	0.00	0.00	0.05	1.39
20TS-02 mgt(4)	0.00	0.00	0.00	0.00	0.06	0.02	71.40	7.33	0.00	0.00	0.00	0.00	0.00	0.00	0.03	0.76
20TS-02 mgt(6)	0.00	0.00	0.00	0.00	0.07	0.04	72.36	7.76	0.00	0.00	0.00	0.00	0.00	0.00	0.03	0.92
20TS-02 mgt(8)	0.00	0.00	0.00	0.00	0.14	0.05	76.19	13.38	0.00	0.00	0.00	0.00	0.00	0.00	0.03	0.72
20TS-02 mgt(9)	0.00	0.00	0.00	0.00	0.10	0.02	73.15	20.11	0.00	0.00	0.00	0.00	0.00	0.00	0.03	0.34
20TS-04.1 mgt(3)	0.00	0.00	0.00	0.00	0.10	0.02	75.12	8.09	0.00	0.00	0.00	0.00	0.00	0.00	0.05	0.48
20TS-04.1 mgt(4)	0.00	0.00	0.00	0.00	0.10	0.01	75.00	6.05	0.00	0.00	0.00	0.00	0.00	0.00	0.05	0.42
20TS-04.1 mgt(5)	0.00	0.00	0.00	0.00	0.08	0.06	77.27	37.24	0.00	0.00	0.00	0.00	0.00	0.00	0.04	1.11
20TS-04.1 mgt(6)	0.00	0.00	0.00	0.00	0.10	0.04	57.12	12.60	0.00	0.00	0.00	0.00	0.00	0.00	0.05	1.03
20TS-04.1 mgt(7)	0.00	0.00	0.00	0.00	0.10	0.03	76.89	23.37	0.00	0.00	0.00	0.00	0.00	0.00	0.05	0.68
20TS-04.1 mgt(8)	0.00	0.00	0.00	0.00	0.11	0.04	77.78	11.31	0.00	0.00	0.00	0.00	0.00	0.00	0.05	0.75
20TS-04.2 mgt(1)	0.00	0.00	0.00	0.00	0.09	0.01	71.86	5.96	0.00	0.00	0.00	0.00	0.00	0.00	0.03	0.38
20TS-04.2 mgt(2)	0.00	0.00	0.00	0.00	0.10	0.01	73.65	6.13	0.00	0.00	0.00	0.00	0.00	0.00	0.03	0.43
20TS-04.2 mgt(5)	0.00	0.00	0.00	0.00	0.10	0.04	63.73	7.32	0.00	0.00	0.00	0.00	0.00	0.00	0.03	1.06
20TS-04.2 mgt(6)	0.00	0.00	0.00	0.00	0.10	0.02	64.95	12.38	0.00	0.00	0.00	0.00	0.00	0.00	0.04	1.12
20TS-04.2 mgt(9)	0.00	0.00	0.00	0.00	0.11	0.02	72.57	8.20	0.00	0.00	0.00	0.00	0.00	0.00	0.04	0.46
20TS-04.2 mgt(10)	0.00	0.00	0.00	0.00	0.09	0.01	70.58	10.45	0.00	0.00	0.00	0.00	0.00	0.00	0.04	0.28
21TS-MB01 mgt	0.00	0.00	0.00	0.00	0.08	0.01	74.74	6.02	0.00	0.00	0.00	0.00	0.00	0.00	0.02	0.51
21TS-MB01 mgt(1)	0.00	0.00	0.00	0.00	0.13	0.02	71.62	5.96	0.00	0.00	0.00	0.00	0.00	0.00	0.01	0.50
21TS-MB01 mgt(2)	0.00	0.00	0.00	0.00	0.07	0.01	68.97	5.77	0.00	0.00	0.00	0.00	0.00	0.00	0.02	0.53
21TS-MB01 mgt(3)	0.00	0.00	0.00	0.00	0.07	0.01	67.74	5.91	0.00	0.00	0.00	0.00	0.00	0.00	0.02	0.60
21TS-MB01 mgt(4)	0.00	0.00	0.00	0.00	0.08	0.01	71.72	6.13	0.00	0.00	0.00	0.00	0.00	0.00	0.02	0.55
21TS-MB02 mgt(1)	0.00	0.00	0.00	0.00	0.10	0.01	70.20	5.32	0.00	0.00	0.00	0.00	0.00	0.00	0.02	0.76
21TS-MB02 mgt(2)	0.00	0.00	0.00	0.00	0.13	0.01	68.26	6.15	0.00	0.00	0.00	0.00	0.00	0.00	0.02	0.85
21TS-MB02 mgt(3)	0.00	0.00	0.00	0.00	0.17	0.04	93.01	10.79	0.00	0.00	0.00	0.00	0.00	0.00	0.03	1.10
21TS-MB02 mgt(4)	0.00	0.00	0.00	0.00	0.08	0.03	75.13	22.66	0.00	0.00	0.00	0.00	0.00	0.00	0.01	0.68
21TS-MB03 mgt1	0.00	0.00	0.00	0.00	0.09	0.01	70.28	6.13	0.00	0.00	0.00	0.00	0.00	0.00	0.01	0.46
21TS-MB03 mgt3	0.00	0.00	0.00	0.00	0.08	0.01	69.63	6.36	0.00	0.00	0.00	0.00	0.00	0.00	0.02	0.40
21TS-MB03 mgt4	0.00	0.00	0.00	0.00	0.10	0.02	68.07	7.73	0.00	0.00	0.00	0.00	0.00	0.00	0.01	0.37
21TS-MB03 mgt5	0.00	0.00	0.00	0.00	0.08	0.01	68.72	6.37	0.00	0.00	0.00	0.00	0.00	0.00	0.01	0.31
21TS-MB03 mgt6	0.00	0.00	0.00	0.00	0.09	0.02	69.49	4.95	0.00	0.00	0.00	0.00	0.00	0.00	0.02	0.40
21TS-MB03 mgt7	0.00	0.00	0.00	0.00	0.09	0.02	71.12	7.44	0.00	0.00	0.00	0.00	0.00	0.00	0.00	0.31

Sample	^{24}Mg	2SD	^{25}Mg	2SD	^{27}Al	2SD	^{29}Si	2SD	^{43}Ca	2SD	^{44}Ca	2SD	^{47}Ti	2SD	^{49}Ti	2SD	^{51}V	2SD
21TS-MB05 mgt1	0.06	0.04	0.06	0.04	0.14	0.06	0.43	0.16	0.18	0.14	0.18	0.11	0.05	0.04	0.05	0.05	0.00	0.00
21TS-MB05 mgt2	0.08	0.05	0.08	0.04	0.19	0.09	0.54	0.19	0.22	0.16	0.21	0.13	0.03	0.01	0.03	0.01	0.00	0.00
21TS-MB05 mgt3	0.11	0.02	0.11	0.01	0.17	0.03	0.64	0.07	0.27	0.18	0.24	0.06	0.03	0.01	0.03	0.01	0.00	0.00
21TS-MB05 mgt5	0.09	0.04	0.09	0.04	0.13	0.06	0.49	0.16	0.17	0.12	0.18	0.09	0.03	0.01	0.03	0.01	0.00	0.00
21TS-MB05 mgt6	0.07	0.04	0.07	0.04	0.12	0.06	0.42	0.23	0.16	0.14	0.16	0.13	0.04	0.04	0.04	0.03	0.00	0.00
21TS-MB06 mgt1	0.17	0.12	0.17	0.13	0.45	0.19	0.69	0.51	0.24	0.26	0.24	0.24	0.02	0.01	0.02	0.01	0.00	0.00
21TS-MB06 mgt2	0.18	0.11	0.18	0.11	0.49	0.19	0.81	0.50	0.28	0.22	0.28	0.15	0.02	0.00	0.02	0.00	0.00	0.00
21TS-MB06 mgt4	0.22	0.05	0.23	0.05	0.44	0.08	1.02	0.29	0.51	0.23	0.52	0.14	0.03	0.01	0.02	0.00	0.00	0.00
21TS-MB06 mgt6	0.18	0.08	0.18	0.07	0.21	0.06	0.95	0.49	0.39	0.25	0.40	0.18	0.02	0.00	0.02	0.01	0.00	0.00
21TS-MB06 mgt7	0.07	0.01	0.08	0.01	0.31	0.04	0.32	0.10	0.11	0.12	0.11	0.06	0.02	0.00	0.02	0.00	0.00	0.00
21TS-MB07 mgt1	0.06	0.02	0.06	0.02	0.21	0.07	0.51	0.25	0.24	0.24	0.25	0.13	0.07	0.02	0.07	0.01	0.01	0.00
21TS-MB07 mgt2	0.14	0.04	0.15	0.04	0.31	0.09	0.67	0.18	0.13	0.09	0.13	0.07	0.05	0.01	0.05	0.01	0.01	0.00
21TS-MB07 mgt3	0.06	0.04	0.07	0.03	0.25	0.12	0.41	0.24	0.13	0.11	0.14	0.06	0.08	0.01	0.08	0.02	0.01	0.00
21TS-MB08 mgt1	0.24	0.06	0.25	0.05	0.56	0.11	1.05	0.31	0.45	0.20	0.47	0.12	0.05	0.01	0.05	0.01	0.00	0.00
21TS-MB08 mgt2	0.23	0.04	0.25	0.05	0.49	0.13	1.09	0.26	0.48	0.18	0.51	0.14	0.05	0.01	0.04	0.01	0.00	0.00
21TS-MB08 mgt3	0.06	0.02	0.07	0.03	0.27	0.07	0.34	0.18	0.09	0.12	0.09	0.09	0.03	0.01	0.03	0.00	0.00	0.00
21TS-MB08 mgt4	0.24	0.05	0.26	0.04	0.37	0.08	1.25	0.30	0.53	0.22	0.53	0.10	0.04	0.01	0.03	0.01	0.00	0.00
21TS-MB08 mgt6	0.32	0.06	0.33	0.05	0.60	0.14	1.77	0.38	0.78	0.29	0.80	0.15	0.03	0.01	0.03	0.01	0.00	0.00
21TS-MB08 mgt7	0.23	0.03	0.24	0.03	0.43	0.06	0.93	0.24	0.30	0.16	0.31	0.09	0.03	0.00	0.02	0.01	0.00	0.00
21TS-MB09 mgt2	0.05	0.02	0.05	0.02	0.22	0.07	0.30	0.18	0.14	0.10	0.17	0.10	0.02	0.01	0.02	0.00	0.00	0.00
21TS-MB09 mgt3	0.05	0.03	0.06	0.03	0.16	0.05	0.32	0.20	0.16	0.15	0.14	0.09	0.02	0.01	0.02	0.00	0.00	0.00
21TS-MB09 mgt5	0.16	0.04	0.17	0.05	0.25	0.06	0.79	0.26	0.38	0.24	0.38	0.16	0.03	0.01	0.03	0.01	0.00	0.00
21TS-MB09 mgt6	0.04	0.03	0.04	0.03	0.10	0.05	0.26	0.18	0.12	0.10	0.11	0.09	0.02	0.01	0.02	0.01	0.00	0.00
21TS-MB10 mgt1	0.09	0.05	0.10	0.04	0.11	0.04	0.70	0.31	0.31	0.20	0.30	0.14	0.05	0.01	0.05	0.02	0.00	0.00
21TS-MB10 mgt2	0.03	0.02	0.04	0.02	0.08	0.04	0.26	0.26	0.10	0.12	0.08	0.09	0.05	0.01	0.05	0.01	0.00	0.00
21TS-MB10 mgt5	0.04	0.02	0.04	0.02	0.12	0.05	0.31	0.25	0.11	0.11	0.10	0.07	0.05	0.02	0.05	0.02	0.00	0.00
21TS-MB10 mgt1.1	0.06	0.05	0.06	0.05	0.12	0.04	0.57	0.38	0.17	0.21	0.16	0.17	0.06	0.01	0.06	0.01	0.00	0.00
21TS-MB10 mgt4.1	0.08	0.09	0.08	0.08	0.18	0.19	0.51	0.36	0.09	0.10	0.09	0.04	0.04	0.01	0.04	0.01	0.00	0.00
sk2ab mgt2	0.17	0.07	0.17	0.07	0.28	0.07	0.80	0.25	0.39	0.43	0.36	0.35	0.01	0.00	0.02	0.00	0.00	0.00
sk2ab mgt4	0.24	0.04	0.24	0.03	0.35	0.06	1.12	0.34	0.42	0.24	0.41	0.13	0.04	0.01	0.04	0.01	0.00	0.00
sk2ab mgt5	0.14	0.03	0.15	0.04	0.25	0.07	0.70	0.15	0.13	0.11	0.14	0.04	0.04	0.01	0.03	0.01	0.00	0.00
sk2ab mgt6	0.19	0.03	0.19	0.03	0.18	0.03	0.93	0.19	0.31	0.13	0.31	0.07	0.04	0.01	0.04	0.01	0.00	0.00
sk2ab mgt7	0.03	0.02	0.03	0.02	0.19	0.02	0.26	0.13	0.03	0.05	0.03	0.03	0.03	0.01	0.03	0.01	0.00	0.00
21TS-DG01b mgt1	0.01	0.00	0.01	0.00	0.16	0.02	0.07	0.09	0.00	0.05	0.01	0.03	0.00	0.00	0.00	0.00	0.00	0.00
21TS-DG01b mgt2	0.00	0.00	0.00	0.00	0.14	0.03	0.08	0.08	0.03	0.08	0.03	0.06	0.01	0.00	0.01	0.00	0.00	0.00
21TS-DG01b mgt3	0.00	0.00	0.00	0.00	0.10	0.02	0.06	0.09	0.00	0.05	0.00	0.03	0.00	0.00	0.00	0.00	0.00	0.00
21TS-DG01b mgt4	0.02	0.01	0.02	0.01	0.12	0.04	0.33	0.12	0.01	0.04	0.01	0.03	0.02	0.01	0.02	0.00	0.00	0.00
21TS-DG01b mgt5	0.04	0.01	0.04	0.01	0.15	0.03	0.42	0.14	0.07	0.07	0.07	0.04	0.02	0.00	0.02	0.01	0.00	0.00
21TS-DG01b mgt6	0.01	0.00	0.01	0.00	0.13	0.02	0.08	0.08	0.01	0.04	0.01	0.04	0.00	0.00	0.00	0.00	0.00	0.00

Sample	^{52}Cr	2SD	^{53}Cr	2SD	^{55}Mn	2SD	^{56}Fe	2SD	^{59}Co	2SD	^{60}Ni	2SD	^{71}Ga	2SD	Ti+V	Al+Mn+Ca
21TS-MB05 mgt1	0.00	0.00	0.00	0.00	0.06	0.01	71.53	7.45	0.00	0.00	0.00	0.00	0.00	0.00	0.06	0.38
21TS-MB05 mgt2	0.00	0.00	0.00	0.00	0.07	0.02	74.96	12.46	0.00	0.00	0.00	0.00	0.00	0.00	0.04	0.48
21TS-MB05 mgt3	0.00	0.00	0.00	0.00	0.08	0.00	75.53	3.29	0.00	0.00	0.00	0.00	0.00	0.00	0.04	0.51
21TS-MB05 mgt5	0.00	0.00	0.00	0.00	0.07	0.01	72.78	6.01	0.00	0.00	0.00	0.00	0.00	0.00	0.03	0.37
21TS-MB05 mgt6	0.00	0.00	0.00	0.00	0.06	0.01	71.90	7.75	0.00	0.00	0.00	0.00	0.00	0.00	0.04	0.35
21TS-MB06 mgt1	0.00	0.00	0.00	0.00	0.14	0.02	71.03	6.85	0.00	0.00	0.00	0.00	0.00	0.00	0.03	0.82
21TS-MB06 mgt2	0.00	0.00	0.00	0.00	0.12	0.02	68.54	6.81	0.00	0.00	0.00	0.00	0.00	0.00	0.02	0.90
21TS-MB06 mgt4	0.00	0.00	0.00	0.00	0.15	0.02	69.44	7.58	0.00	0.00	0.00	0.00	0.00	0.00	0.03	1.10
21TS-MB06 mgt6	0.00	0.00	0.00	0.00	0.06	0.01	69.20	5.56	0.00	0.00	0.00	0.00	0.00	0.00	0.03	0.66
21TS-MB06 mgt7	0.00	0.00	0.00	0.00	0.11	0.01	65.92	5.57	0.00	0.00	0.00	0.00	0.00	0.00	0.03	0.53
21TS-MB07 mgt1	0.00	0.00	0.00	0.00	0.06	0.01	68.05	5.41	0.00	0.00	0.00	0.00	0.00	0.00	0.08	0.52
21TS-MB07 mgt2	0.00	0.00	0.00	0.00	0.05	0.01	70.17	8.23	0.00	0.00	0.00	0.00	0.00	0.00	0.06	0.49
21TS-MB07 mgt3	0.00	0.00	0.00	0.00	0.04	0.01	64.85	9.53	0.00	0.00	0.00	0.00	0.00	0.00	0.09	0.42
21TS-MB08 mgt1	0.00	0.00	0.00	0.00	0.15	0.02	69.47	7.07	0.00	0.00	0.00	0.00	0.00	0.00	0.05	1.16
21TS-MB08 mgt2	0.00	0.00	0.00	0.00	0.13	0.03	63.29	6.79	0.00	0.00	0.00	0.00	0.00	0.00	0.05	1.10
21TS-MB08 mgt3	0.00	0.00	0.00	0.00	0.10	0.02	65.55	6.94	0.00	0.00	0.00	0.00	0.00	0.00	0.03	0.46
21TS-MB08 mgt4	0.00	0.00	0.00	0.00	0.12	0.01	67.58	5.66	0.00	0.00	0.00	0.00	0.00	0.00	0.04	1.02
21TS-MB08 mgt6	0.00	0.00	0.00	0.00	0.15	0.02	67.04	7.37	0.00	0.00	0.00	0.00	0.00	0.00	0.03	1.53
21TS-MB08 mgt7	0.00	0.00	0.00	0.00	0.15	0.01	67.18	5.50	0.00	0.00	0.00	0.00	0.00	0.00	0.03	0.87
21TS-MB09 mgt2	0.00	0.00	0.00	0.00	0.08	0.03	79.69	6.12	0.00	0.00	0.00	0.00	0.00	0.00	0.02	0.44
21TS-MB09 mgt3	0.00	0.00	0.00	0.00	0.06	0.02	72.75	9.29	0.00	0.00	0.00	0.00	0.00	0.00	0.02	0.37
21TS-MB09 mgt5	0.00	0.00	0.00	0.00	0.08	0.01	71.73	7.10	0.00	0.00	0.00	0.00	0.00	0.00	0.03	0.71
21TS-MB09 mgt6	0.00	0.00	0.00	0.00	0.04	0.01	69.69	8.38	0.00	0.00	0.00	0.00	0.00	0.00	0.02	0.26
21TS-MB10 mgt1	0.00	0.00	0.00	0.00	0.07	0.01	67.89	6.52	0.00	0.00	0.00	0.00	0.00	0.00	0.06	0.49
21TS-MB10 mgt2	0.00	0.00	0.00	0.00	0.06	0.01	70.35	8.70	0.00	0.00	0.00	0.00	0.00	0.00	0.05	0.24
21TS-MB10 mgt5	0.00	0.00	0.00	0.00	0.08	0.02	71.16	6.38	0.00	0.00	0.00	0.00	0.00	0.00	0.05	0.31
21TS-MB10 mgt1.1	0.00	0.00	0.00	0.00	0.09	0.01	71.86	7.32	0.00	0.00	0.00	0.00	0.00	0.00	0.06	0.37
21TS-MB10 mgt4.1	0.00	0.00	0.00	0.00	0.05	0.01	68.13	3.55	0.00	0.00	0.00	0.00	0.00	0.00	0.05	0.32
sk2ab mgt2	0.00	0.00	0.00	0.00	0.14	0.04	68.86	5.65	0.00	0.00	0.00	0.00	0.00	0.00	0.01	0.80
sk2ab mgt4	0.00	0.00	0.00	0.00	0.14	0.02	72.30	13.53	0.00	0.00	0.00	0.00	0.00	0.00	0.04	0.91
sk2ab mgt5	0.00	0.00	0.00	0.00	0.15	0.03	63.59	7.16	0.00	0.00	0.00	0.00	0.00	0.00	0.04	0.53
sk2ab mgt6	0.00	0.00	0.00	0.00	0.12	0.03	76.26	7.07	0.00	0.00	0.00	0.00	0.00	0.00	0.04	0.61
sk2ab mgt7	0.00	0.00	0.00	0.00	0.10	0.01	70.20	5.50	0.00	0.00	0.00	0.00	0.00	0.00	0.03	0.32
21TS-DG01b mgt1	0.00	0.00	0.00	0.00	0.08	0.01	73.94	7.56	0.00	0.00	0.00	0.00	0.00	0.00	0.00	0.24
21TS-DG01b mgt2	0.00	0.00	0.00	0.00	0.06	0.01	71.03	7.68	0.00	0.00	0.00	0.00	0.00	0.00	0.01	0.22
21TS-DG01b mgt3	0.00	0.00	0.00	0.00	0.07	0.01	74.62	4.97	0.00	0.00	0.00	0.00	0.00	0.00	0.00	0.16
21TS-DG01b mgt4	0.00	0.00	0.00	0.00	0.06	0.01	72.37	7.63	0.00	0.00	0.00	0.00	0.00	0.00	0.02	0.19
21TS-DG01b mgt5	0.00	0.00	0.00	0.00	0.08	0.01	69.47	9.29	0.00	0.00	0.00	0.00	0.00	0.00	0.03	0.30
21TS-DG01b mgt6	0.00	0.00	0.00	0.00	0.08	0.00	70.52	4.89	0.00	0.00	0.00	0.00	0.00	0.00	0.00	0.23